FLUID MIXING LASERS*

Terrill A. Cool

Laboratory of Plasma Studies
Cornell University
Ithaca, New York 14850

Abstract

The use of rapid gasdynamic mixing in high speed flow systems for creating population inversions in molecular laser systems is discussed for the cases of electrical excitation followed by selective energy transfer and for excitation by chemical reaction. A summary and discussion is given of recent experimental results concerning electrically and chemically excited fluid mixing lasers. A brief discussion is given of the first chemical laser to operate continuously with no external source of energy, by the simple mixing together of commercially available bottled gases.

---

*Prepared under NASA Contract NGL-33-010-064.

Manuscript submitted to I.R. Schwenker for proceedings of NASA Conference on Gas Lasers July 15, 16, (1968).

I. Introduction

There are at present an ever increasing number of laser systems which fit naturally under the broad classification "fluid mixing lasers". For these lasers, the rapid mixing together of fluids is an essential feature of the laser pumping process, or of the relaxation mechanism for the lower laser level, or of both. To date, this class of lasers has been confined to completely gaseous systems, but it may eventually be extended to include potentially important cases for which mixing is accomplished by a rapid initial dispersal of liquid droplets within a gas followed by a rapid subsequent vaporization or "flashing" of the droplets.

Until quite recently, the best examples of fluid mixing lasers [1-4] have been based upon the N_2-CO_2 or N_2-N_2O laser systems originally demonstrated and developed by Patel [5,6] and independently proposed by Legay and co-workers [7,8]. These lasers achieve pumping of the upper laser level through the selective transfer of vibrational-rotational energy by the mixing of vibrationally excited N_2 with initially unexcited CO_2 or N_2O. For such lasers effective operation depends upon the achievement of a characteristic mixing time that is less than the vibrational relaxation time for the upper laser level [2,9]. It is possible, however, to achieve limited operation for much slower rates of mixing* provided, of course, that mixing is accomplished before significant vibrational-translational energy relaxation can occur in the initially excited nitrogen

---

* It is interesting to note in this context that fluid mixing laser action was successfully demonstrated for the helium-neon atomic system by achieving mixing rates only fast enough to exceed the initial de-excitation rates for helium (2^3S) metastables convected downstream from an electrical discharge, despite the fact that there was no possibility for achievement of mixing rates comparable to the de-excitation rate for the upper laser level in neon[10].

molecules, as Patel's early experiments [5,6] demonstrate.

During this past summer of 1969, significant progress has been made in the chemical laser field. Continuous-wave chemical laser action was reported simultaneously by two groups working independently on different chemical systems [11,12]. These first cw chemical lasers operating in the HF and HCl-CO_2 molecular systems were pumped by vibrational energy released from chemical reactions; however, an additional energy source was required for initial partial dissociation of reactants. These systems were quickly followed by two new cw chemical lasers operating in the DF-CO_2 and HF-CO_2 molecular systems [13].

A long awaited milestone was reached in August with the successful demonstration of laser operation by purely chemical means; no additional energy source, thermal or electrical, was necessary [14]. Continuous-wave chemical laser operation in CO_2 at 10.6 microns was achieved in the DF-CO_2 system solely by the simple mixing of bottled gases. It is expected that work currently underway at several laboratories will quickly lead to other purely chemical cw lasers operating by means of the rapid mixing of reactants.

Because of these recent developments, the author has felt it desirable to extend somewhat the discussion relating to chemical laser systems originally presented at the NASA Gas Laser Conference of July 15-16, 1968. Because of continuing practical interest in the electrically excited N_2-CO_2 fluid mixing laser, some discussion will be given of our work on this system with emphasis on material originally presented at the Conference, but not yet published elsewhere.

II. Fluid Mixing Laser Configurations

Figure 1 schematically illustrates the concept of one possible type of

fluid mixing laser. The flow moves in the positive Z-direction between two partially reflecting mirrors (not shown) aligned so that the optical axis lies parallel to the X-axis, transverse to the flow direction[9,15,16]. Rapid mixing of a secondary gas with the primary gas flow is accomplished by introducing the secondary gas by means of small jets located along adjacent airfoils fed by manifold arrays. A simplified version of the airfoil-manifold array of Figure 1 (a single bank of 16 airfoils with 12 orifices of .028 in. dia.) has been used quite successfully to inject CO_2 into a primary flow of vibrationally excited N_2 mixed with He[2]. Simplified airfoils consisting of perforated round tubes also work well, and injection in lateral directions instead of downstream is sometimes convenient. In our chemical laser work, we have found it necessary to cover perforated stainless steel injector tubes with Teflon to avoid surface recombination losses of atomic species.

Figure 2 shows schematically a fluid mixing laser for which the optical axis is aligned along the flow direction. We have successfully used this type of configuration for preliminary studies of the electrically excited N_2-CO_2 laser system (unpublished) as well as for studies of various chemical laser systems [12-14]. For this configuration, a secondary flow is introduced into the primary flow by means of a Teflon injector located at the upstream end of the Teflon reaction tube. Mixing and injection is accomplished by means of orifices located in the side walls. The mixing system of Figure 2 is quite useful for small scale fundamental studies of laser systems, but cannot be readily scaled up in size in contrast to the configuration of Figure 1. Most of the laser output for the configuration of Figure 2 is contributed from that portion of the flow within the Teflon reaction tube[13]. The dimensions of this tube are determined by considerations of the maximum permissible cavity diffraction losses, of the maximum permissible pressure drop along the tube, and of the need for a minimum characteristic mixing time.

Several authors have recently reported interesting results on flowing gas laser systems operating with either a transverse optical axis (as in Figure 1), or with a longitudinal optical axis (as in Figure 2) with respect to the flow direction[1,3,17,18]. Very high power densities have been obtained in such flow lasers both with and without fluid mixing[1,17,18].

III. Gain Measurements in the N_2-CO_2 Fluid Mixing Laser

Several features of fluid mixing lasers of practical importance have been recently studied with the electrically excited N_2-CO_2 laser system. Before discussing this work, it will be desirable to mention briefly several of the advantages of high speed flow lasers generally, both with and without fluid mixing. The phrase "high speed flow laser" used here is meant to apply to those lasers for which characteristic flow transit times are much less than the characteristic times for the diffusion of the component species to the walls of the device.[2,16]

Patel [5] realized that the possibility of obtaining a laser with a gain that is approximately independent of tube diameter was inherent in the CO_2 laser system. That is, for CO_2 lasers and for molecular lasers operating on vibrational-rotational transitions generally, volume collisional relaxation effects can dominate spontaneous emission and diffusion in contrast to atomic gaseous lasers. Until rather recently, however, the N_2-CO_2 laser has conventionally been operated under conditions such that surface dependent effects (heat conduction, diffusion, wall recombination of ions) have had a substantial effect upon the gains and ultimate power outputs available from such systems. In fact, the concept of separately exciting molecules in a discharge and then subsequently mixing them with CO_2 to produce laser action that Patel originally employed was largely abandoned in favor of the use of premixed, slowly flowing gases. This neglect

of the fluid mixing N_2-CO_2 laser was perhaps as much because the early experiments on this system [5,6] were done with apparatus incapable of adequately demonstrating the inherent advantages of the fluid mixing concept, as it was because of the simplicity of the conventional premixed system for small scale applications. At present, it appears that the advantages of molecular laser systems employing high speed flowing gases, with and without fluid mixing, are beginning to be realized in the design of high power laser oscillators and amplifiers [1,17,18].

High-speed flowing gas lasers offer many advantages, as has been discussed by several authors: [2,3,9,10,15-21]

1. A uniform and low translational gas temperature can be maintained by rejecting unusable energy (as heat) with the exhausting flow. Conventional lasers are constrained by the requirement that heat be lost at the wall surfaces. For conventional lasers, the gas temperature and lower state laser population are, therefore, determined to a large extent by the surface-dependent method of heat rejection; consequently, the gain is not independent of tube diameter and the power output cannot be scaled with tube diameter.

2. Conventional lasers have electron densities that have a maximum value at the tube axis but fall to zero at the tube walls because the primary loss mechanism for ions in the discharge is by surface recombination. In a flow laser, on the other hand, convective losses of ions can be dominant and a more uniform electrical excitation is, in principle, possible.

3. High-speed flows permit the use of gas dynamic expansion techniques for the achievement of uniform and low translational and rotational gas temperatures. Such techniques enable the direct utilization of thermal energy sources.

4. The use of high-speed flows and rapid fluid mixing provide a means to accomplish an uncoupling of excitation processes from relaxation processes to

allow their independent optimizations.

5. The uncoupling of (4), above, can be used to provide for the use of a variety of excitation techniques by electrical, thermal, or chemical means.

6. Selective relaxation of the lower laser level can be accomplished by the injection and mixing of a selected additive gas to preferentially quench the lower laser level (e.g., by increasing the vibration-translation relaxation rate for the lower CO_2 laser-level by the addition of helium).

7. Many of the above features are responsible for gain saturation and power output characteristics that are substantially different for flowing gas lasers in comparison with conventional lasers [9]. The high-speed flow enables a very large convective flux of molecular vibrational energy to be maintained within the laser cavity (e.g., because of higher operating pressures, improved excitation methods, uncoupling of excitation from relaxation, etc.). For flow lasers operating at pressures above a few torr [9], the effective "mean flow laser saturation parameter" can substantially exceed the saturation parameter for conventional lasers.

8. A properly designed high-speed flow laser (negligible boundary layer thickness, uniform translational temperature, etc.) can provide a uniformly high gain that is independent of dimensions transverse to the flow direction.

Because of the present lack of data concerning excitation and relaxation processes in high-speed flow laser systems, a series of experiments were performed with an electrically excited fluid mixing N_2-CO_2 laser amplifier. The objective of these experiments was to obtain basic data concerning the following points:

(A) What are the magnitudes of single-pass unsaturated gain coefficients that can be realized in an electrically excited N_2-CO_2 system, if uniform mixing can be accomplished on a time scale shorter than the characteristic time for

vibrational relaxation of the upper CO_2 laser level?

(B) Is it possible to achieve a uniformly high gain, independent of dimensions transverse to the flow, in high-speed CO_2 flow lasers as originally suggested by Patel [5] ?

(C) Can the relaxation processes subsequent to the mixing process be calculated accurately from first principles with available rate coefficient data?

(D) What are reasonable values of the "initial conditions" (population densities, temperatures) to assign for calculations of electrically excited fluid-mixing laser performance for an optical cavity with a transverse axis located just downstream of the mixing zone?

(E) Can rapid mixing techniques be used conveniently for the direct quantitative measurement of vibrational relaxation rates of interest in laser applications?

Figure 4 shows schematically how a CO_2 laser oscillating on the P(18) transition at 10.57 μ was employed as a probe to measure the single-pass small-signal gain in a fluid-mixing CO_2 laser amplifier. A diffraction grating of 150 line/mm blazed at 8 μ was mounted as one mirror of the oscillator to provide laser oscillation on individual vibration-rotation transitions[22]. The output mirror of the probe laser was mounted within a piezoelectric element which enabled the resonator length to be varied to bring the oscillating frequency of the cavity resonance in coincidence with the center frequency of the gain profile of the flowing gas in the fluid mixing system. Note that the center frequency of the gain curve in the high-speed flowing gas of the fluid mixing system is slightly Doppler shifted with respect to the center frequency of the unsaturated gain curve of the probe laser. The measurement technique has been described previously[22].

Measurements were made by detecting the chopper modulated and collimated output of the probe laser beam after it passed through the length L of the fluid-mixing system. The power ratio, exp ($\bar{\alpha}$L), was measured as the ratio of detected output power with CO_2 mixing into the flow to that with no CO_2 present in the flow.

Figure 5 indicates how the injection airfoil array appeared as viewed from downstream. For these experiments both 2.54-cm-I.D. and 5.1-cm-I.D. Pyrex flow tubes were employed. For the 2.54-cm-I.D. flow tube, 16 airfoils with 12 injection orifices (0.028-in-diam) were used; for the 5.1-cm-I.D. flow tube, 14 airfoils with 14 injection orifices (0.046-in-diam) were used. The gap separating airfoils was about 0.040-in for the 2.54-cm-I.D. tube and 0.045-in for the 5.1-cm-I.D. tube. Only a small circular cross section (0.040-in-diam) of the total (0.125-in-diam) collimated probe laser beam passing directly between the two adjacent central airfoils was allowed to reach the detector.

Measurements of gain coefficients,

$$\bar{\alpha} = \frac{1}{L} \int_0^L \alpha \, dZ \ ,$$

averaged along the mixed flow length L were made for various lengths L for flow tubes of both diameters. The radial profile of average gain coefficients for a given flow length L was determined by translating both the probe laser beam and detection optics across the tube diameter to permit observations at various beam positions between the two adjacent central airfoils.

Figure 6 shows the way $\int_0^L \alpha \, dZ$ depends on the length L for measurements made along the tube axis with gas compositions that maximized the gain for a 1-m flow length. Excitation conditions were identical for tubes of a given diameter, but we estimate that because of a higher nitrogen flow rate for the 5.1-cm-I.D. tubes that the average vibrational energy per nitrogen

molecule leaving the discharge was about 25% less than in the 2.54-cm-I.D. case. This accounts for the lower asymptotic value for $\bar{\alpha}$ L for large L with the 5.1-cm-I.D. Notice the very high average gain coefficients we obtain; for example, for a 2.54-cm-I.D. and L = 18.5 cm, $\bar{\alpha}$ = 4.15 cm^{-1} (for conventional CO_2 lasers of 2.54-cm-I.D., [22] $\alpha \lesssim 1.0\ m^{-1}$).

Figure 7 shows a typical radial profile of the average gain coefficient normalized by the centerline value for a 2.54-cm-I.D. tube with L = 1 m (the solid and dashed curves are the result of theoretical calculations yet to be discussed). Data (not shown) for a 5.1-cm-I.D. tube of the same length exhibit a flat central region of uniformly high gain extending to larger values of r/r_o than for the 2.54-cm-I.D. case. Radial profile measurements such as those of Figure 7 were made at each of the flow lengths, L, corresponding to the positions at which data points are given in Figure 6. The data of Figs. 6 & 7 (with minor corrections for varying pressure drops for the differing flow lengths) can be used to infer the local gain coefficient values at any point in the flow.

The data of Figures 6 and 7 were taken under optimum conditions giving a maximum average gain as measured along the axis of a 1 m length of a given diameter tube. The data of Figures 8 to 11 illustrate the method of optimization as applied to the 2.54-cm-I.D. tube. Figure 8 shows the variation in the average gain coefficient with helium partial pressure for fixed N_2 and CO_2 partial pressures. Since the optimum helium partial pressure of about 3 torr did not change substantially for moderate variations in CO_2 and N_2 partial pressures, it was possible to set the helium pressure at 3 torr and find the optimum operating conditions by examination of the influences of variations in CO_2 concentration for several fixed N_2 partial pressures. This is illustrated by Figures 9 to 11. Figure 9 shows the variations in average gain coefficient as a function of CO_2 partial pressure for three representative values of N_2 partial pressure for a helium partial pressure of 3.05 torr. Using

the maximum gain coefficients as obtained from curves such as given in Figure 9 a curve of optimum gain coefficient (for the optimum CO_2 partial pressure corresponding to a given N_2 partial pressure) as a function of N_2 partial pressure can be plotted as shown in Figure 10 . Figure 11 shows the data presented in a perhaps more meaningful fashion. Here a well defined optimum ratio of CO_2 to N_2 partial pressure is indicated which decreases approximately linearly with N_2 partial pressure for moderate variations in N_2 partial pressure about 1 torr. The maximum value of optimized gain coefficient occurs for the partial pressures: N_2 = 0.85 torr, CO_2 = 1.70 torr, and He = 3.05 torr.

We have been able to verify by theoretical calculations to be described in the following that the variations of Figures 8 to 11 are satisfactorily explained qualitatively in terms of the various collisional vibrational energy transfer processes connecting the vibrational levels of CO_2 which occur in the presence of N_2, CO_2 and He. The detailed comparison of experiment and theory for the gas composition changes represented by Figures 8 to 11 will be presented elsewhere. It is interesting to examine here the comparison of the experimental axial and radial average gain profiles (Figures 6 and 7) with theory.

Theoretical calculations have been performed for the relaxing flows downstream from the mixing zone by assuming that a uniform velocity profile and uniform mixing of components exists near the injector ($\lesssim$ 2-cm downstream)*.

---

* That is, uniform mixing is assumed to be accomplished in about 100 microseconds. This time corresponds approximately to the characteristic time for diffusive mixing of these flows with initial stratifications of about 1 mm. The flow area at the plane of injectors for the primary flow has been chosen so that the primary flow is nearly sonic as it passes between the airfoils to promote uniform velocity conditions, but a uniform velocity profile is probably only approximately achieved.

Because the characteristic time for vibrational energy transfer from N_2 to CO_2 is less than the characteristic mixing time under the conditions of these experiments, the maximum gain values are reached just downstream of the injectors ($\sim$2 cm) at the cross sectional plane where uniform mixing is accomplished. The populations of the various vibrational levels in CO_2 have been calculated for all points downstream of this plane of uniform mixing by specifying the velocity and the vibrational populations at this initial position. The initial flow velocity is known and the initial population densities may be readily estimated from the experimentally determined axial variation in average gain coefficient as given in Figure 6 *. More accurate initial populations may then be obtained by choosing those initial values which give a best fit between experiment and theory for the axial variation in average gain coefficients.

The theoretical model used for such calculations includes the effects of the diffusion of vibrational energy within a multicomponent mixture, of viscous boundary layer development, and of the various collisional vibrational relaxation processes. The theory has been developed within the framework of approximations afforded by the assumption of an isothermal incompressible flow.**

---

* Notice how potentially useful this type of graph is. The ordinate divided by the abcissa at each position, L, along the curve gives the average gain coefficient, $\bar{\alpha} = \frac{1}{L}\int_0^L \alpha \, dZ$, at this position. Also the slope of the curve of $\bar{\alpha}L$ as a function of L gives the local gain coefficient α.

**Under severe conditions, the pressure drop along the flow can reach 45%, and the temperature rise can be as high as 70°K. Fortunately, in most cases the extent of the interesting region of significant optical gain does not extend far enough along the flow to invalidate the analysis.

Only the results of such calculations will be given here, as the details will be presented elsewhere [23].

Figure 12 compares the variation in gain coefficients, averaged over the flow length L for a 2.54-cm-I.D. tube, as determined by two separate experimental methods with theory. The solid data points correspond to those given in Figure 6.

The open data points of Figure 12 were determined from measurements of the intensity of the 4.3 μ emission band from the (00°1) vibrational level of CO_2 made at various infrared transmitting side windows located at various positions along the flow. The relative variation in the upper CO_2 laser state (00°1) is given directly from these measurements. Because the translational temperature of these experiments is quite low (330°K) compared to the effective vibrational temperature of the upper laser level (10^3 - 10^4°K), and because of the efficient vibrational-translation coupling of the lower laser level afforded by the presence of a substantial fraction of helium in the flow, the population of the lower laser level is quite low (effective vibrational temperature $\lesssim$ 400°K). Therefore, only a small correction for the lower state population is necessary to calculate the variation in local gain coefficient along the flow directly from the measured variation in the 4.3 μ emission intensity. The averaged gain coefficients, plotted as the open points in Figure 12, are then determined by integration of the local gain coefficient along the flow.

The solid curve of Figure 12 corresponds to a theoretical calculation using rate coefficients that give a best fit with the two sets of experimental data. The overall relaxation rate for a best fit is approximately 70% larger than that calculated with currently accepted values [24,25] of rate coefficients for measured pressures and temperatures of our experiments. This discrepancy

is perhaps partially caused by the effects of nitrogen atoms and of various excited species of nitrogen present in the flow *. Perhaps another explanation lies in the fact that the temperature dependence of the rate coefficients changes rapidly near our experimental conditions; either uncertainties in the measured rates in this temperature region [24], or a small underestimate of our gas temperature could account for the discrepancy.

The solid theoretical curve shown with the data of Figure 7 was calculated according to the aforementioned procedure. The agreement between experiment and theory is probably as good as could be expected with the approximations that have been made in the present analysis. The primary effect producing the nonuniform average gain profile as a function of the radial coordinate is caused by the developing viscous boundary layer. The theoretical calculations indicate that the effect of diffusion toward the walls induced by the nonuniformities created by the boundary layer is not a major loss mechanism for vibrationally excited states for the tube diameters used here.

To illustrate this point, Figure 7 shows a calculation (dashed curve) for which the effects of diffusion are not included (the diffusion coefficient has been set equal to zero). The rather small influence of diffusion relative to that of the developing viscous boundary layer demonstrated by these curves has its origin in the relatively rapid rates of collisional relaxation of the vibrational levels as a loss mechanism for vibrational energy compared with the rate at which energy diffuses from a given region of the flow. The cumulative action of the boundary layer in slowing the particle velocities below that of the central uniform core allows very substantial relative differences in population to develop at a given location downstream because

---

* Under conditions of reduced power input to the upstream discharge, we have measured rate coefficients that agree reasonably well with those of other experimenters [23].

the progress of collisional relaxation is greatest for those flow regions most influenced by the slowly moving boundary layer.

It is clear from the foregoing discussion and from the experimental data presented in Figures 7 and 12 that, except for those regions of the flow substantially influenced by boundary layer development, the vibrational state populations (and hence the gain) depend primarily upon volume collisional processes*. Thus, it is possible to build laser systems for which a uniformly high gain can be achieved for very large transverse flow dimensions. The laser power output of such high speed flow systems can be scaled (except for gain saturation effects along the optical axis) with transverse flow dimensions[2,9].

Figure 13 shows how the local small-signal gain coefficient, α, varies along the flow direction** if mixing is assumed to be accomplished instantaneously at the origin, Z = 0. The gain grows very rapidly at first during the initial energy transfer process from vibrationally excited N_2 to initially unexcited CO_2. The gain reaches a maximum when the net loss rate of energy by collisional transfer from the upper CO_2 laser level has increased to balance the net rate of pumping from the nitrogen. The gain then decays relatively slowly at a rate limited by the overall collisional relaxation rate for the upper laser level as coupled to the reservoir of vibrational energy contained in the nitrogen[9,25]. The dashed line on Figure 13 represents the location at which mixing is complete in these experiments.

For actual laser operation with a transverse optical axis, the influence of cavity radiation upon the relaxation of vibrational populations is quite important and can produce relaxation characteristics substantially different from those discussed above[9].

---

*However, stimulated emission and absorption processes can have pronounced effects upon vibrational state populations.

**The distance along the flow direction has been nondimensionalized by using the coordinate $Z^* = Z/r_o R_e$, where Z is distance along the flow direction, r_o is the flow tube radius, and R_e is the Reynolds number for the flow defined in terms of the tube radius.

IV. A Purely Chemical Laser

We have recently reported the first successful operation of a chemical laser for which cw laser output was achieved solely by the simple act of mixing bottled gases together [14]. Continuous-wave operation in CO_2 at 10.6 microns has been achieved without the use of electrical or thermal energy sources.

The important steps in the mechanism for chemical pumping of CO_2 were the following:

A. A source of fluorine atoms was provided by mixing nitric oxide with a flowing mixture of fluorine and helium, as a result of the reaction

$$F_2 + NO \rightarrow ONF + F \qquad (1)$$

B. The combined flows were then rapidly mixed with deuterium and carbon dioxide to produce vibrationally excited DF by the chain reaction

$$F + D_2 \rightarrow (DF)^* + D \qquad (2a)$$

$$D + F_2 \rightarrow (DF)^* + F \qquad (2b)$$

followed by the intermolecular transfer of vibrational-rotational energy from DF to CO_2,

$$DF(v=n) + CO_2(00^\circ0) \rightarrow DF(v=n-1) + CO_2(00^\circ1) \; . \qquad (3)$$

Figure 14 shows a schematic diagram of the fluid mixing chemical laser. The apparatus was similar to that of Figure 2 except that no RF discharge was necessary. Step A, above, occurred in an 11-mm-I.D. quartz sidearm tube leading into the main flow laser tube as shown. The rapid mixing of step B, above, was accomplished by an injector located at the upstream end of a 21 cm length of 9 mm bore Teflon reaction tube. Mixing and reaction took place

quite rapidly (100-200 μ sec) in the high speed (600 m/sec) flow passing through the Teflon reaction tube; the major portion of the laser output was contributed from this portion of the flow [13]. The flow left the Teflon reaction tube at sonic velocity and expanded to flow another 60 cm along the 2.54-cm-I.D. Pyrex flow tube before being exhausted into a sidearm tube. All interior wall surfaces of the flow laser were coated with H_3BO_3 according to the method of Ogryzlo [26].

Laser power output was measured for the optical cavity of Figure 14 with the use of calibrated 10.6 micron attenuators and a calibrated Eppley thermopile. A maximum power output of 0.23 watts was observed for this DF-CO_2 laser at the partial flow rates: F_2 = 390 μ moles/sec, He = 3830 μ moles/sec, NO = 19 μ moles/sec, D_2 = 360 μ moles/sec, and CO_2 = 1570 μ moles/sec. Under these conditions, the pressure just upstream of the Teflon reaction tube was 19 torr. The pressure dropped along the Teflon reaction tube to a value of about 6.7 torr (65% less than the upstream value)[13] just before the flow entered the expansion region. The pressure in the expanded flow was 1.0 torr.

Figures 15 and 16 show the relative variation in the DF-CO_2 laser output caused by respective variations in each of the partial flow rates, as observed with a bolometer and tuned amplifier. The variations in each of the partial flow rates were performed while holding the other flows constant at approximately the values given above. The flow rates for each of the gases have been normalized by the optimum flow rate value for that gas.

Several additional chemical reactions giving vibrationally excited DF, HF, and HCl have been found to produce laser action at 10.6 μ. Table I summarizes performance data obtained with the flow laser system of Figure 2. It is expected that other reactions giving rise to vibrationally excited HBr or HI should also give cw laser action (e.g., $H + Br_2 \rightarrow HBr + Br$, $Br + HI \rightarrow HBr + I$, $H + I_2 \rightarrow HI + I$).

It should be emphasized that all of the chemical laser work discussed here has been performed with optical cavities designed to have low losses. The power outputs have been found to be substantially increased in several cases over the values recorded here by using mirrors of higher transmittance. For practical laser operation at high powers, a transverse optical system has many advantages [9,15,16].

Chemically pumped CO_2 lasers of the type considered here are theoretically capable of high efficiencies of conversion of the energy of chemical reaction into laser energy. For example, consider the purely chemical laser of reactions (1) to (4) in the foregoing discussion. An efficiency (as described above) of nearly 10% is predicted with the following assumptions:

(a) A stoichiometric chain reaction of D_2 and F_2 can be sustained by providing a 6 percent excess of F_2 for reaction with NO by reaction (1).

(b) Half of the available chemical energy of the overall reaction $D_2 + F_2 \rightarrow 2DF$ is realized as vibrational energy of DF.

(c) CO_2 has a quantum efficiency of 38 percent.

(d) Half of the vibrational energy of $(DF)^*$ is lost by competing processes.

Such a "chemical efficiency" compares very favorably with the "electrical efficiency" of large scale N_2-CO_2 electrically excited flow lasers [17]. The comparison is even more favorable if the overall thermodynamics of the generation of the electrical energy consumed by the N_2-CO_2 system is considered.

V. Gasdynamic Mixing Behind Shock Waves

Accepting the proposition that further study of rapid fluid mixing techniques is important in the development of large scale cw molecular lasers, one then must inquire as to the means by which such mixing might be accomplished. Several ideas for augmenting ordinary laminar or turbulent diffusive mixing

suggest themselves, e.g.,

A. The secondary components can be mixed with the primary gas by initial dispersion by droplet injection, followed by a rapid induced vaporization and diffusive mixing in the gas phase. There appear to be many ways to induce the rapid vaporization of the droplets. These might include: vaporization by thermal radiation, injection of highly positively charged droplets into a primary plasma to take advantage of enhanced mixing due to electrostatic effects and droplet vaporization by the release of surface recombination energy, vaporization enhanced by droplet breakup due to resonances driven by oscillating acoustic and electrical fields, etc.

B. Rotating flows can provide extremely high accelerations to drive the mixing of gaseous components of differing densities.

C. Ultrasonic, electrostatic, and electromagnetic oscillations may be useful in inducing breakup of gaseous interfaces.

D. Magnetogasdynamic interactions could aid in mixing ionized gases.

However, the need for mixing of large volumes of gases in short times places a fundamental constraint upon the selection of possible techniques. That is, mixing across interfacial surfaces of limited extent, even though accomplished in acceptably short times, cannot provide the high volume rates of mixing that "volume" type mixing techniques (i.e., not essentially limited by the effective interfacial surface area) could provide. Ideas such as the droplet injection scheme or the use of electrostatic oscillations, etc., though conceivably providing the essential means to produce violent breakup of interfaces and to provide the desired volume rates of mixing, would require restrictive selections for the types of gases to be mixed and of their physical states. The volume mixing rates achievable by jet-mixing or rotating-flow mixing appear to be "surface limited" and attempts to overcome this limitation appear to involve complicated orifice arrangements that are difficult to build (see

Figure 1) and tend to promote excessive destruction of requisite species by surface de-excitation or recombination.

For these several reasons, the simplicity of the technique, and its potential for the introduction of violent interfacial instabilities, the shock mixing concept discussed by the author at the NASA Gas Laser Conference is considered here in connection with some recent experimental results.

An interesting phenomenon, apparently well known but not extensively studied, occurs when an initially nonuniform or stratified flow passes through a shock wave. The shock can interact with the flow to abruptly cause instabilities to occur at the interfaces between those regions which prior to the shock have appreciably different components of momentum normal to the shock wave. The form of the instabilities can be of the Taylor type if initial flow stratifications exist parallel to the plane of the shock, or of the Kelvin-Kelmholtz type for the case where the initial planes of stratification are normal to the plane of the shock.

Such instabilities are coupled with large pressure inequalities, flow reversal, and vortex formation that can be generated by the shock wave interaction with the stratified flow. These features may have important application to the problem of the achievement of rapid mixing of laminar flows. In this case, the shock can serve as a means to violently break up the flow stratifications and thereby reduce the characteristic length for diffusive mixing as well as increase the effective interfacial area across which diffusion occurs. The resultant increase in volume mixing rates would probably be not unlike that attending the abrupt transition from laminar to turbulent flow. As has been mentioned, the inherent causes for such unstable recirculating flows are the initial momentum differences between portions of the flow upstream of the shock. These differences can be produced by density differences or velocity differences, or both. The gasdynamic literature contains many references to the above types of phenomena, but apparently no serious proposals have been

advanced for the direct use of such shock wave - fluid flow interactions as a means to achieve rapid volume mixing in gases. This use was suggested to the author by F. K. Moore some time ago [27].

Examples of references to the above phenomena can be cited in connection with problems in supersonic combustion [28-32], shock wave interactions with flame fronts [33-38], with boundary layers [39-43], with wakes and wake turbulence [44-46], with jets [47-48], with bubbles [28], with density stratifications [49], and with shock wave interactions with liquid flows and layers [50], etc. Despite such references to the occurance of enhanced mixing behind shocks, apparently no explicit studies of the mixing process itself have been undertaken.

Figure 17 shows the essential features of the gasdynamic shock-mixing process taken from a schlieren photograph [51] of a shock wave moving into an initially stratified air-helium gas system. Figure 17 shows the interaction process in shock fixed coordinates that was observed after an initial transient period as the shock moved through the stratified gas ahead of it. Viewed in shock-fixed coordinates, the central lamina of helium approached at an upstream Mach number of 1.2; the surrounding air approached at a Mach number of 3.5*. The upstream pressure and temperature were 80 torr and 300°K respectively. The shock structure consists of segments of normal shocks that exist at the outer edges of the air flow and across the central lamina of helium. A bifurcated "foot" consisting of two oblique shocks connects the outer air flow and the central helium flow across an inner region of air flow. Similar shock bifurcations have been observed in shock-boundary layer interactions [41-43]. The helium

---

* The flow situation pictured is achieved in a shock tube by providing a thin sandwich of helium gas enclosed by very delicate lacquer membranes separating the inner helium gas from the surrounding air. The membranes are about 1000 A° thick, prepared according to the general technique developed by Jahn [49].

passes through the normal shock and expands subsonically outward presenting a wedge-shaped boundary along which the bounding supersonic air flow slips past. Along this interface a Kelvin-Helmholtz instability develops due to the large velocity slip between these adjacent flows. The helium contained within this wedge-shaped boundary expands subsonically and mixes with the outer flow in a clearly defined region labeled "mixing zone" in Figure 17. In this region of rapid mixing the vorticity generated along the bounding helium-air interface is markedly amplified. This highly rotational flow region connects the relatively high pressure outer airflow in the regions A and B of Figure 17 to the relatively low pressure helium flow existing in the region C . This difference in pressures between these unmixed portions of the overall flow is caused by the large momentum difference between the entering flows because of the relatively small mass of helium as compared with that of air. The static pressure of the air flow in regions A and B is about1130 torr compared with a stagnation pressure of 212 torr for the helium flow in region C . There is thus no possibility for the helium to leave region C except by rapidly mixing with a portion of the air flow in the mixing zone so that the total pressure of the mixed flows is sufficient to "match" with the remaining unmixed outer air flow.

Stated another way, a portion of the air flow passing through the bifurcated oblique shock "foot" is "sacrificed" so that by mixing this portion of the outer flow with the lower pressure helium flow, the mixed flows are able to proceed downstream with the unmixed portions of the outer air flow. This is possible by virtue of the fact that the thus "sacrificed" portion of the air flow has a higher total pressure than that of the outer air flow passing through the normal shock.

Eventually this rotational mixing region diffuses outward to envelop the entire flow and uniformly mixed conditions are achieved further downstream. The

schlieren photographs we have obtained to date [51] indicate that no large density gradients exist in the flow immediately downstream of the mixing zone indicated in Figure 17. Diffusive mixing is doubtless incomplete until somewhat further downstream than the mixing zone indicated in Figure 17; the boundaries of this zone merely indicate that no density gradients are visible beyond this region on our schlieren photographs.

A theoretical analysis of the "gas-mixing shock" of Figure 17 and additional experimental results are being prepared for publication elsewhere, but it is clear from the features of Figure 17 that a pronounced increase in mixing rate occurs for the shocked flows as contrasted with the rates of diffusive mixing of unshocked flows of similar upstream configuration. The shock has produced an enhanced mixing rate by performing irreversible work on the flows resulting in an enormous increase in interfacial area and a resultant increased rate of interdiffusion on a molecular scale.

Figure 18, presented at the Conference, illustrates how this technique might be applied in a fluid mixing chemical laser. The stratified flows immediately upstream of the shock wave system are at a low temperature and little reaction occurs, if at all, before the shock. Immediately behind the shock rapid mixing and reaction occur. The elevated temperatures produced behind the shock may be useful in initiating reactions by supplying the requisite translational activation energy for reaction. Reaction thus occurs in a detonation-like wave leading to population inversion and laser action. In some cases, it may be desirable to provide an expansion region to reaccelerate the flow immediately following the reaction region to cool the gas and enhance or create population inversions. Such an expansion region following the reaction region might also provide a means for the utilization of chemical reactions in which products are close to thermal equilibrium in the reaction zone. This would be a thermally pumped laser for which the thermal energy is supplied by chemical reaction.

Acknowledgement

The author wishes to acknowledge the essential assistance of his graduate students, John B. Barber, John A. Shirley, and Ronald R. Stephens, in obtaining the experimental results that have been discussed here in brief.

References

1. Bronfin, B.R., Boedeker, L.R., and Cheyer, J.P., "Thermal Laser Excitation by Gas Dynamic Mixing in Supersonic Flow", Bull. Am. Phys. Soc. 14, 857(1969).
2. Cool, T.A., and Shirley, J.A., Appl. Phys. Letters 14, 70 (1969).
3. Deutsch, T.F., Horrigan, F.A., and Rudko, R.I., Appl. Phys. Letters 15, 89 (1969).
4. Wisniewski, E.E., Fein, M.E., Verdeyen, J.T., and Cherrington, B.E., Appl. Phys. Letters 12, 257 (1968).
5. Patel, C.K.N., Phys. Rev. Letters 13, 617 (1964).
6. Patel, C.K.N., Appl. Phys. Letters 6, 12 (1965).
7. Legay, F., and Barchewitz, P., Compt. Rend. 256, 5305 (1963).
8. Legay, F. and N. Legay-Sommaire, Compt. Rend. 259, 99 (1964).
9. Cool, T.A., J. Appl. Phys. 40, 3563 (1969).
10. Cool, T.A., Appl. Phys. Letters 9, 418 (1966).
11. Spencer, D.J., Jacobs, T.A., Mirels, H., and Gross, R.W.F., "A Continuous-Wave Chemical Laser", Int. J. of Chem. Kinetics, to be published, Sept., (1969).
12. Cool, T.A., Stephens, R.R. and Falk, T.J., "A Continuous-Wave Chemically Excited CO_2 Laser", Int. J. of Chem. Kinetics, to be published, Sept.,(1969).
13. Cool, T.A., Falk, T.J., and Stephens, R.R., "DF-CO_2 and HF-CO_2 Continuous-Wave Chemical Lasers", Appl. Phys. Letters, to be published.
14. Cool, T.A. and Stephens, R.R., "A Chemical Laser by Fluid Mixing", J. Chem. Phys., to be published, December 1, (1969).
15. Hurle, I.R., and Hertzberg, A., Phys. Fluids 8, 1601 (1965).
16. Wilson, J., Appl. Phys. Letters 8, 159 (1966).
17. Tiffany, W.B., Targ, R., and Foster, J.D., Appl. Phys. Letters 15, 91 (1969).

34. Markstein, G.H., "Flow Disturbances Induced near a Slightly Wavy Contact Surface, or Flame Front, Traversed by a Shock Wave," J. Aero. Sci., 24, 238, (1957).

35. Markstein, G.H., "A Shock Tube Study of Flame Front Pressure Wave Interaction," Sixth Symposium (International) on Combustion, 387-398, New York: Reinhold, (1957).

36. Markstein, G.H., and Schwartz, D., "Interaction between Pressure Waves and Flame Fronts," Jet Propulsion, 25, 174, (1955).

37. Rudinger, G., "Shock Wave and Flame Interactions," Combustion and Propulsion, 153-182, Third AGARD Coll. London: Pergamon, (1958).

38. Laderman, A.J., Urtiew, P.A., and Oppenheim, A.K., "Gas Dynamic Effects of Shock-Flame Interactions in an Explosive Gas," AIAA J. 3, 876, (1965).

39. Griffith, W.C., "Interaction of a Shock Wave with a Thermal Boundary Layer," J. Aero. Sci., 23, 16-22, 66, (1956).

40. Hess, R.V., "Interaction of Moving Shocks and Hot Layers," NACA TN-4002, (1957).

41. Mark, H., "The Interactions of a Reflected Shock Wave with the Boundary Layer in a Shock Tube," Ph.D. Thesis, Cornell University, (1957), also NACA TM-1418 (March, 1958).

42. Dyner, H.B., "Density Variation Due to Reflected Shock-Boundary Layer Interaction", Phys. Fluids, 9, 879 (1966).

43. Davies, L. and Wilson, S.L., "Influence of Reflected Shock and Boundary-Layer Interaction on Shock-Tube Flows", Phys. Fluids 12, Supplement I, I-37, (1969).

44. Ribner, H.S., "Convection of a Pattern of Vorticity through a Shock Wave," NACA TN 2864, (1953).

45. Ribner, H.S., and Moore, F.K., "Unsteady Interaction of Disturbances with a Shock Wave, with Applications to Turbulence and Noise," 1953 Heat Transfer and Fluid Mechanics Institute, Stanford University Press.

46. Kovasnay, L.S.G., "Interaction of a Shock Wave and Turbulence," 1955, Heat Transfer and Fluid Mechanics Institute, UCLA.

47. Dosanjh, D.S., "Experiments on Interaction between a Traveling Shock Wave and a Turbulent Jet," J. Aeronautical Sci., 24, 838-844, (1957).

48. Weeks, T.M. and Dosanjh, D.S., "Interaction between an Advancing Shock Wave and Opposing Jet Flow," AIAA J. 1, 1527-1533, (1963).

49. Jahn, R.G., J. Fluid Mechanics 1, 457 (1956).

50. Borisov, A.A., Kogarko, S.M., and Lyubimov, A.V., "Ignition of Fuel Films behind Shock Waves in Air and Oxygen," preprint for Eleventh Symposium (International) on Combustion (1967).

51. Barber, J.B., "An Experimental Investigation of the Interaction between Laminae of two Gases Passed through a Shock Wave", M.S. Thesis, Cornell University (1969).

Figure Captions

Figure 1 : Schematic Diagram of Fluid Mixing Laser with Transverse Optical Axis

Figure 2 : Schematic Diagram of Fluid Mixing Laser Used for Small Scale Laboratory Studies

Figure 3 : Experimental Arrangement for Unsaturated Gain Measurements on Single Vibrational-Rotational Transitions of a Fluid Mixing CO_2 Laser Amplifier

Figure 4 : Injection Airfoil Array as Viewed from Downstream

Figure 5 : Dependence of the Integrated Gain Coefficient, $\bar{\alpha}L$, Measured Along the Tube Axis, Upon Mixed Flow Length L.

Figure 6 : Radial Profile of the Average Gain Coefficient Normalized by the Centerline Value

Figure 7 : Dependence of the Average Gain Coefficient on Helium Partial Pressure for a Flow Tube with L = 1 m and a 2.54-cm-i.d.

Figure 8 : Dependence of the Average Gain Coefficient on CO_2 Partial Pressure for a Flow Tube with L = 1 m and a 2.54-cm-i.d.

Figure 9 : Dependence of Optimum Average Gain Coefficient Upon Nitrogen Partial Pressure for a Flow Tube with L = 1 m and a 2.54-cm-i.d.

Figure 10: Dependence of Optimum Average Gain Coefficient Upon the Ratio of CO_2 to N_2 Partial Pressures for a Flow Tube with L = 1 m and a 2.54-cm-i.d.

Figure 11: Dependence of the Average Gain Coefficient, $\bar{\alpha}$ Measured Along the Tube Axis, upon Mixed Flow Length L

Figure 12: Variation of the Local Gain Coefficient, α, upon Nondimensional Distance Along the Flow Tube

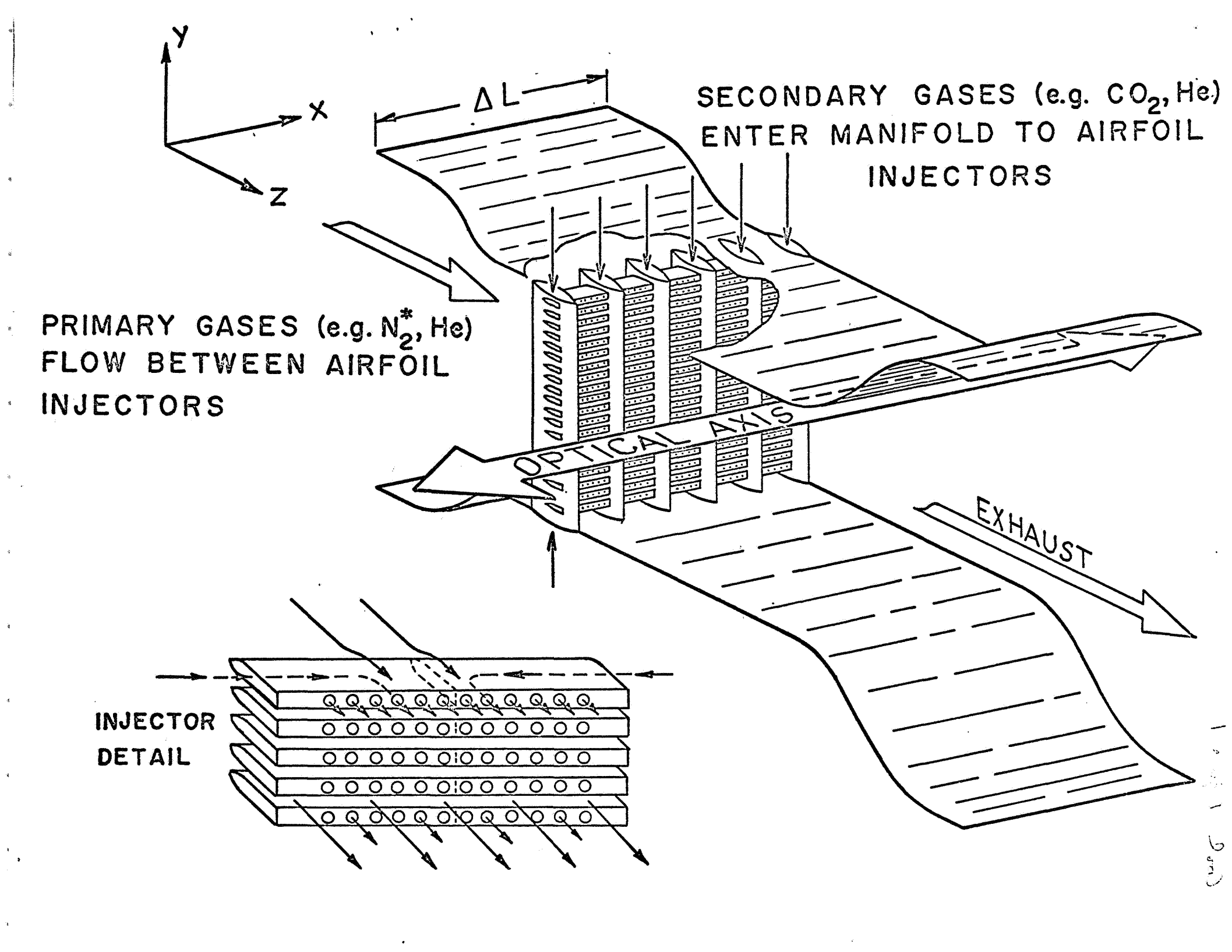
y
x
z
ΔL
SECONDARY GASES (e.g. CO_2, He)
ENTER MANIFOLD TO AIRFOIL
INJECTORS
PRIMARY GASES (e.g. N_2^*, He)
FLOW BETWEEN AIRFOIL
INJECTORS
OPTICAL AXIS
EXHAUST
INJECTOR
DETAIL

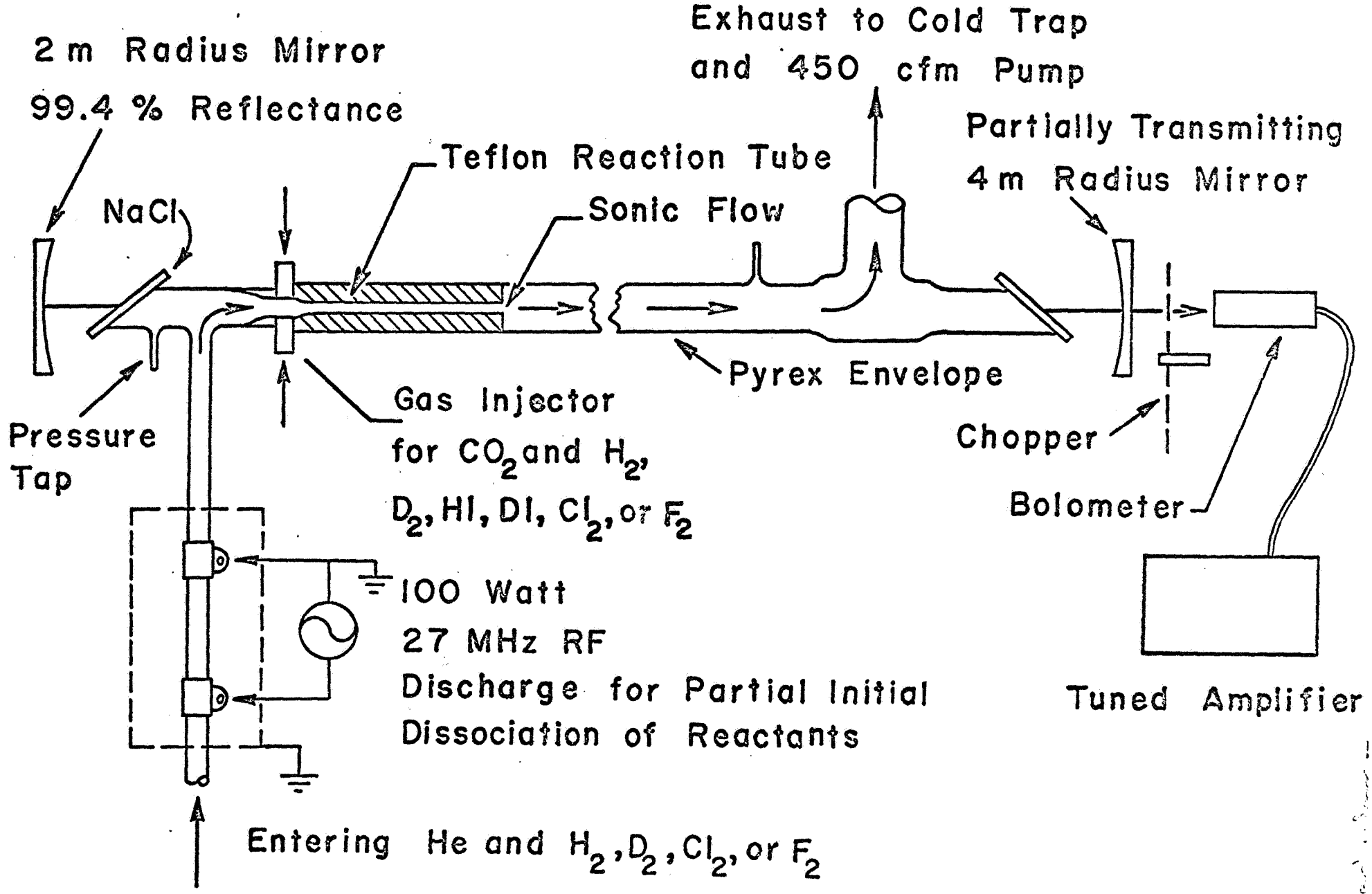
2 m Radius Mirror
99.4 % Reflectance
Exhaust to Cold Trap
and 450 cfm Pump
Partially Transmitting
4 m Radius Mirror
Teflon Reaction Tube
Sonic Flow
NaCl
Pyrex Envelope
Pressure
Tap
Gas Injector
for CO_2 and H_2,
D_2, HI, DI, Cl_2, or F_2
Chopper
Bolometer
100 Watt
27 MHz RF
Discharge for Partial Initial
Dissociation of Reactants
Tuned Amplifier
Entering He and H_2, D_2, Cl_2, or F_2

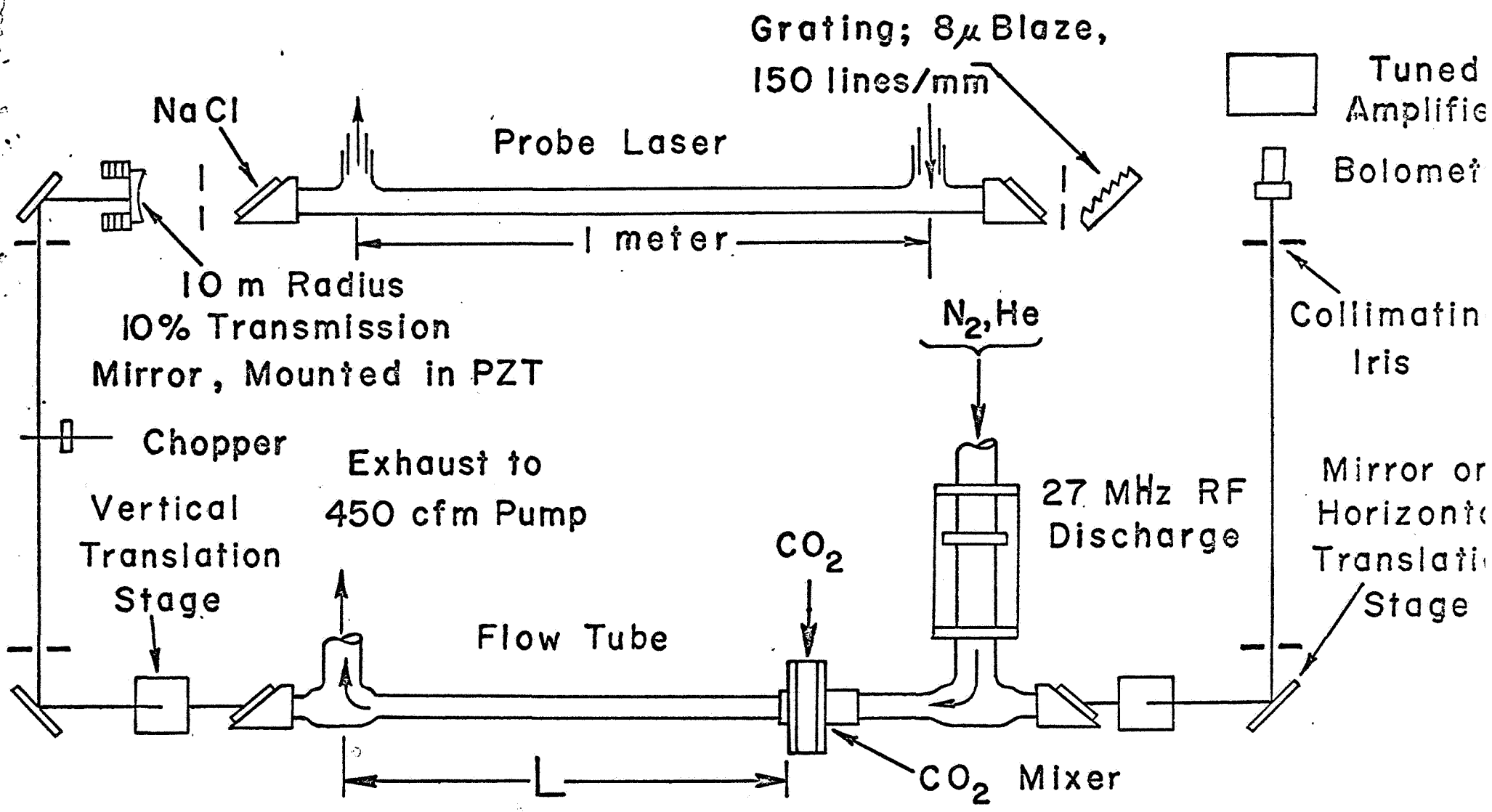
Grating; 8μ Blaze,
150 lines/mm
NaCl
Probe Laser
Tuned
Amplifie
Bolomet
1 meter
10 m Radius
10% Transmission
Mirror, Mounted in PZT
N2,He
Collimatin
Iris
Chopper
Exhaust to
450 cfm Pump
27 MHz RF
Discharge
Mirror or
Horizonte
Translati
Vertical
Translation
Stage
CO2
Flow Tube
Stage
L
CO2 Mixer

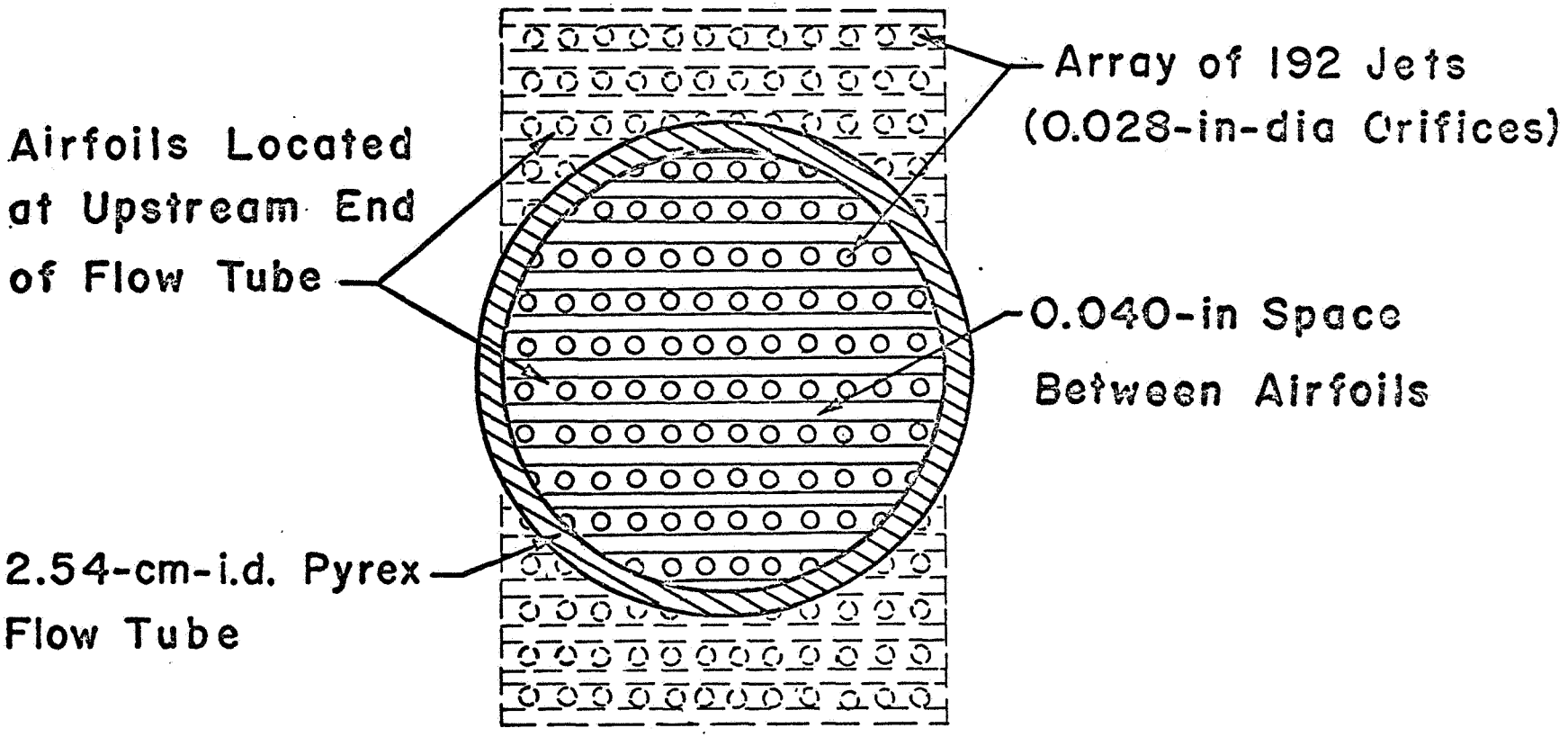

JET MIXING CONFIGURATION

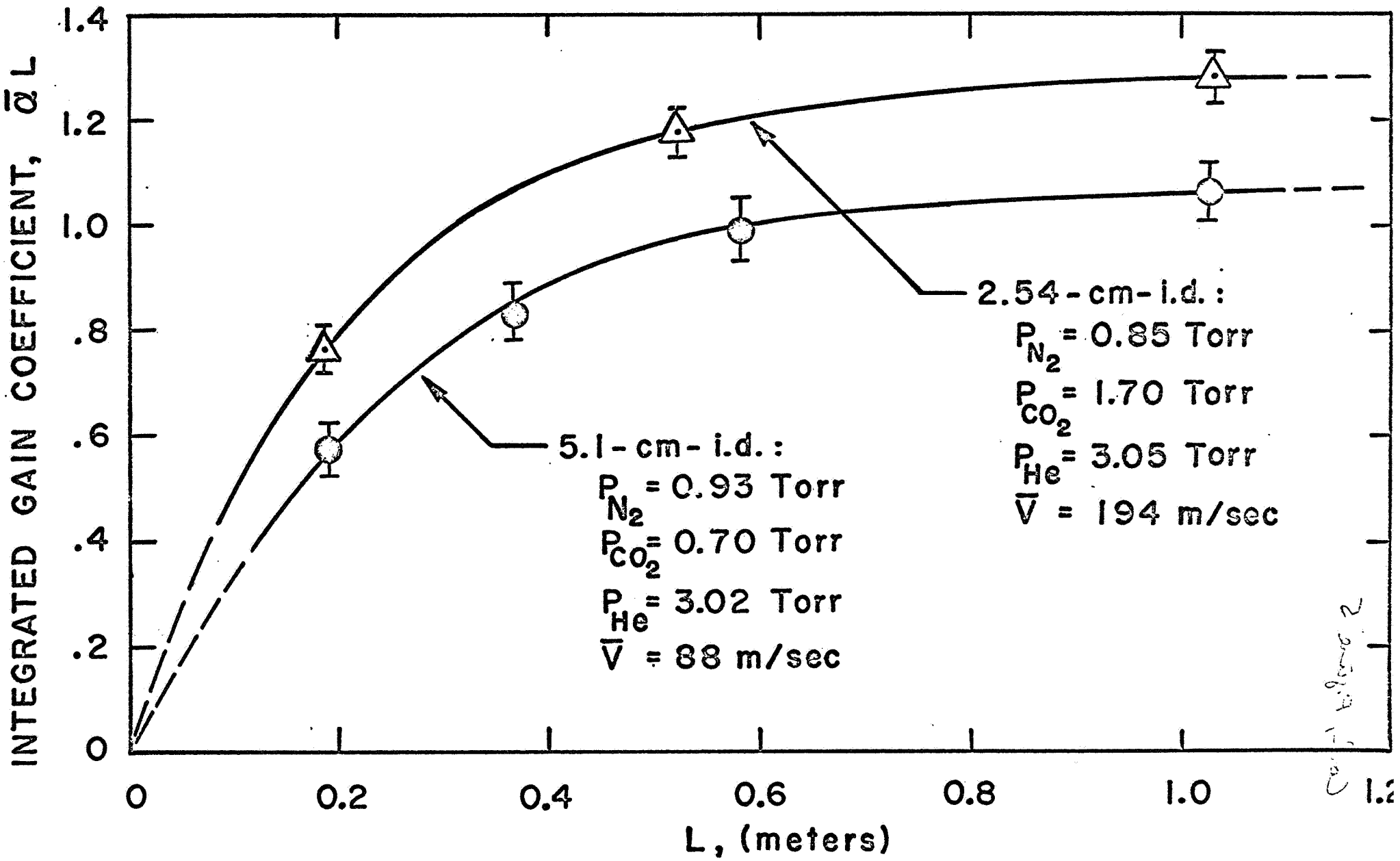
INTEGRATED GAIN COEFFICIENT, $\bar{\alpha}L$
1.4
1.2
1.0
.8
.6
.4
.2
0
0
0.2
0.4
0.6
0.8
1.0
1.2
L, (meters)
2.54-cm-i.d.:
P_{N_2} = 0.85 Torr
P_{CO_2} = 1.70 Torr
P_{He} = 3.05 Torr
$\bar{V}$ = 194 m/sec
5.1-cm-i.d.:
P_{N_2} = 0.93 Torr
P_{CO_2} = 0.70 Torr
P_{He} = 3.02 Torr
$\bar{V}$ = 88 m/sec

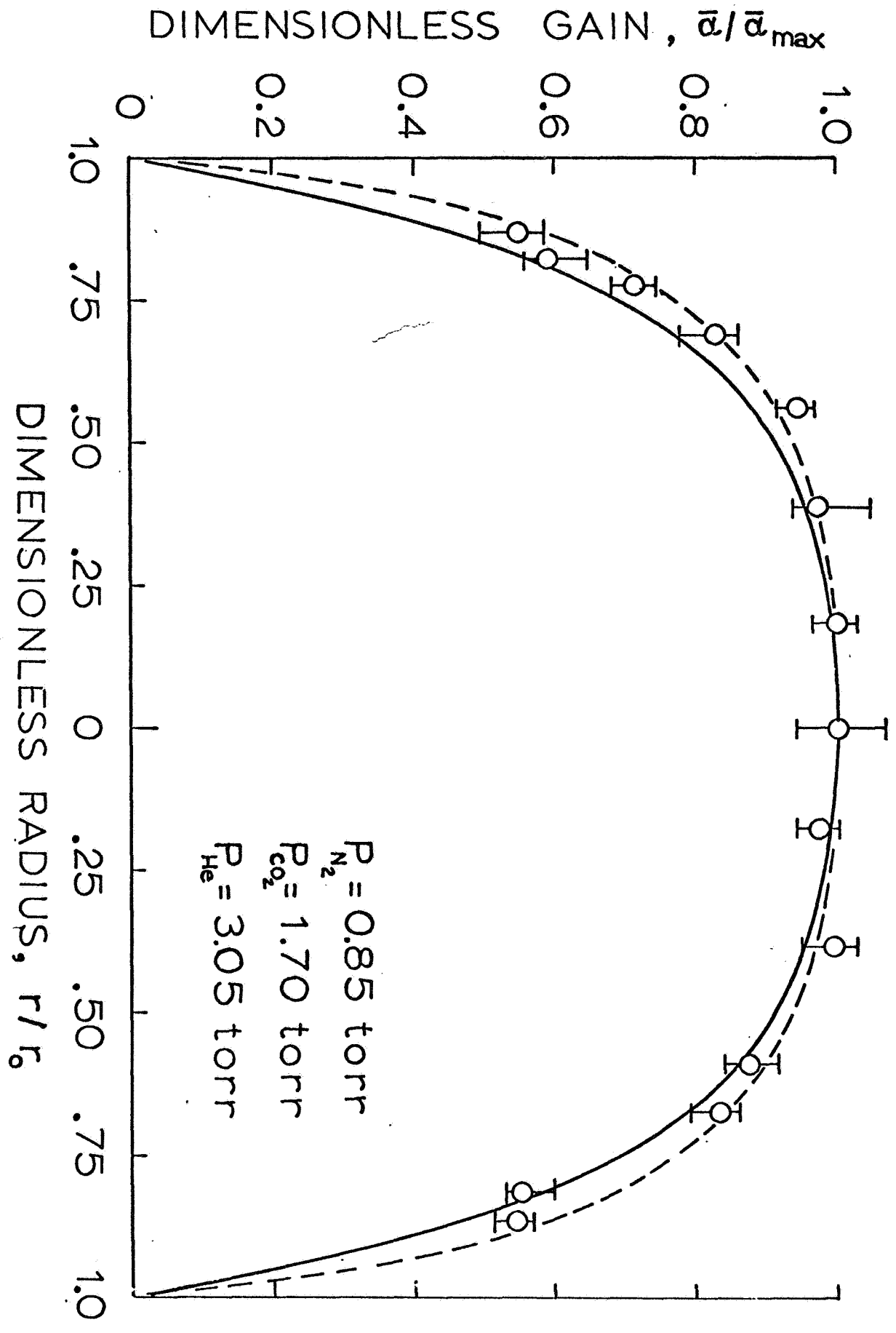
DIMENSIONLESS GAIN, $\bar{\alpha}/\bar{\alpha}_{max}$
0
0.2
0.4
0.6
0.8
1.0
DIMENSIONLESS RADIUS, r/r_o
1.0
.75
.50
.25
0
.25
.50
.75
1.0
P_{N_2} = 0.85 torr
P_{CO_2} = 1.70 torr
P_{He} = 3.05 torr

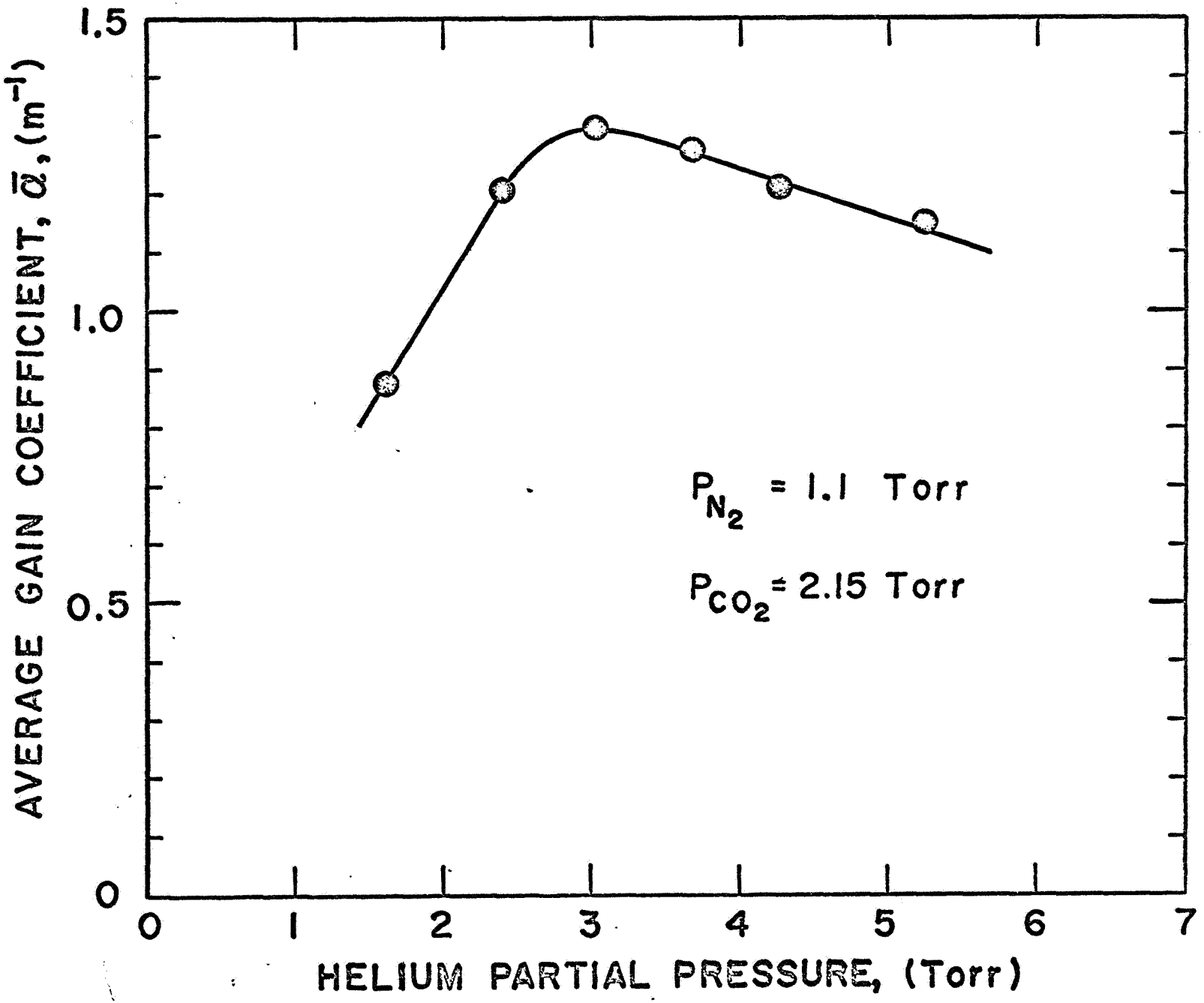
AVERAGE GAIN COEFFICIENT, $\bar{\alpha}$, (m^{-1})
1.5
1.0
0.5
0
0
1
2
3
4
5
6
7
HELIUM PARTIAL PRESSURE, (Torr)
P_{N_2} = 1.1 Torr
P_{CO_2} = 2.15 Torr

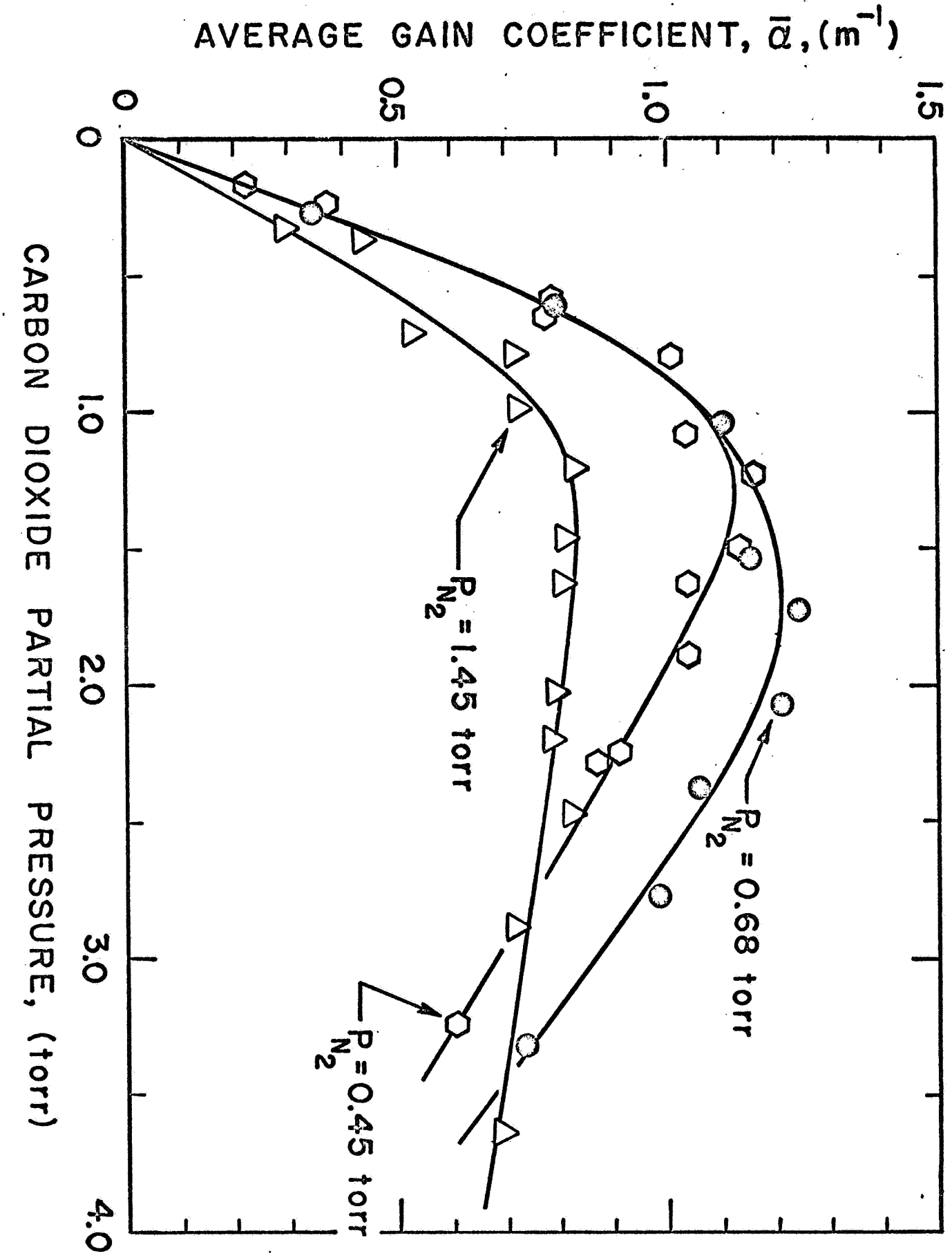
AVERAGE GAIN COEFFICIENT, $\bar{\alpha}$, (m^{-1})
0
0.5
1.0
1.5
CARBON DIOXIDE PARTIAL PRESSURE, (torr)
0
1.0
2.0
3.0
4.0
P_{N_2} = 1.45 torr
P_{N_2} = 0.68 torr
P_{N_2} = 0.45 torr

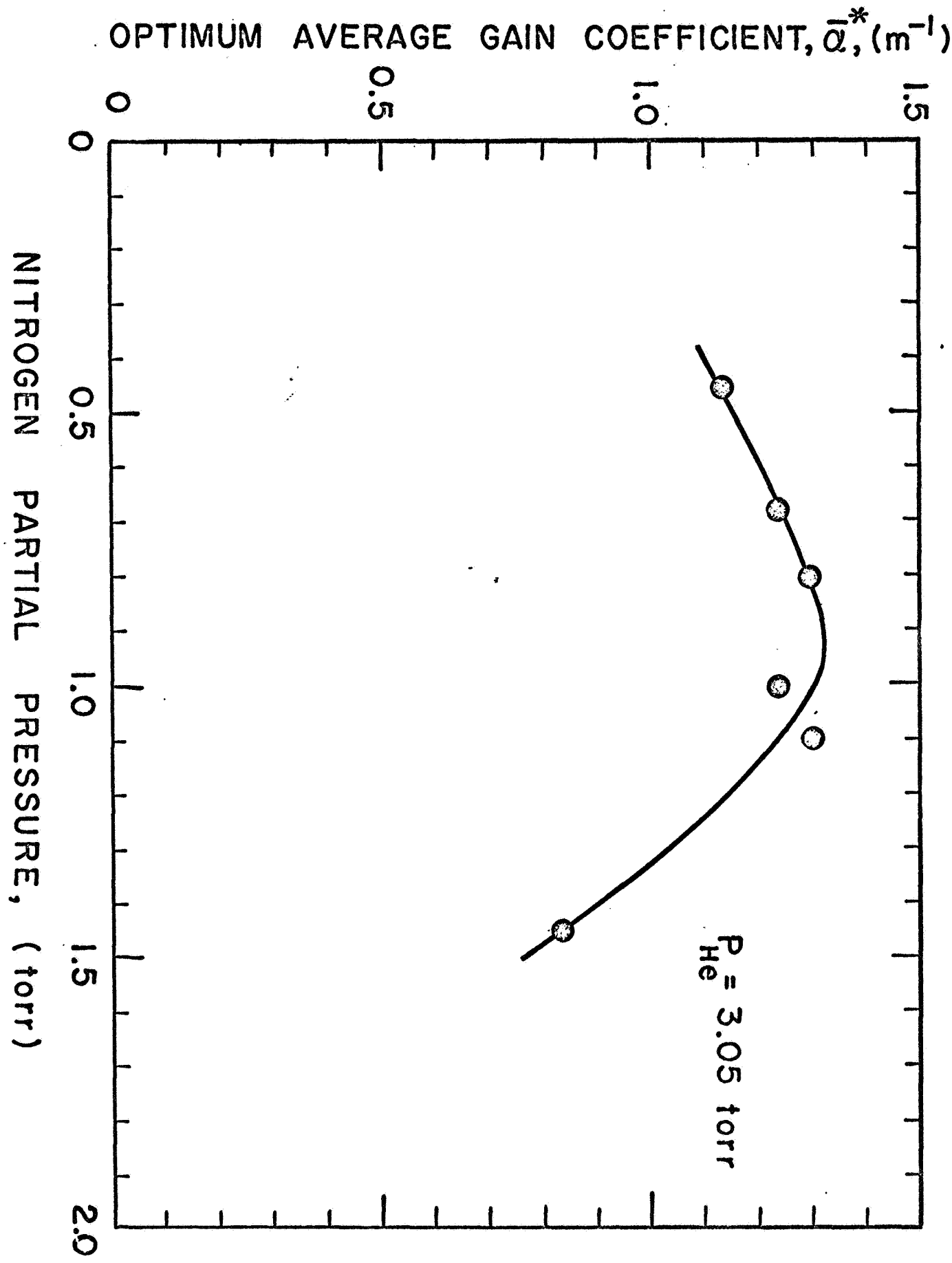
OPTIMUM AVERAGE GAIN COEFFICIENT, $\bar{\alpha}^*$, (m^{-1})
0
0.5
1.0
1.5
NITROGEN PARTIAL PRESSURE, (torr)
0
0.5
1.0
1.5
2.0
P_{He} = 3.05 torr

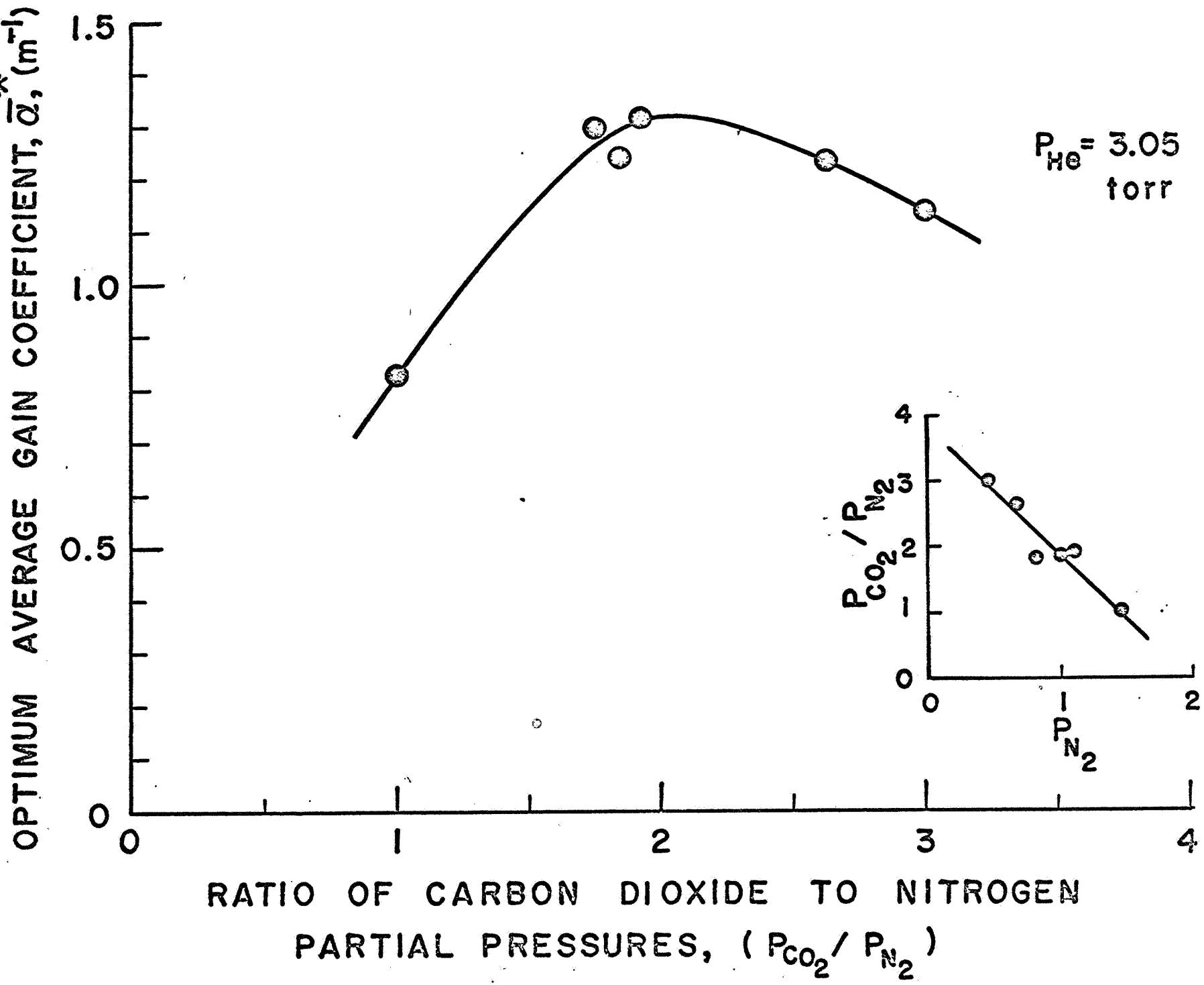
OPTIMUM AVERAGE GAIN COEFFICIENT, $\bar{\alpha}^*$, (m^{-1})
1.5
1.0
0.5
0
0
1
2
3
4
P_{He}= 3.05 torr
P_{CO_2} / P_{N_2}
4
3
2
1
0
0
1
2
P_{N_2}
RATIO OF CARBON DIOXIDE TO NITROGEN PARTIAL PRESSURES, (P_{CO_2} / P_{N_2})

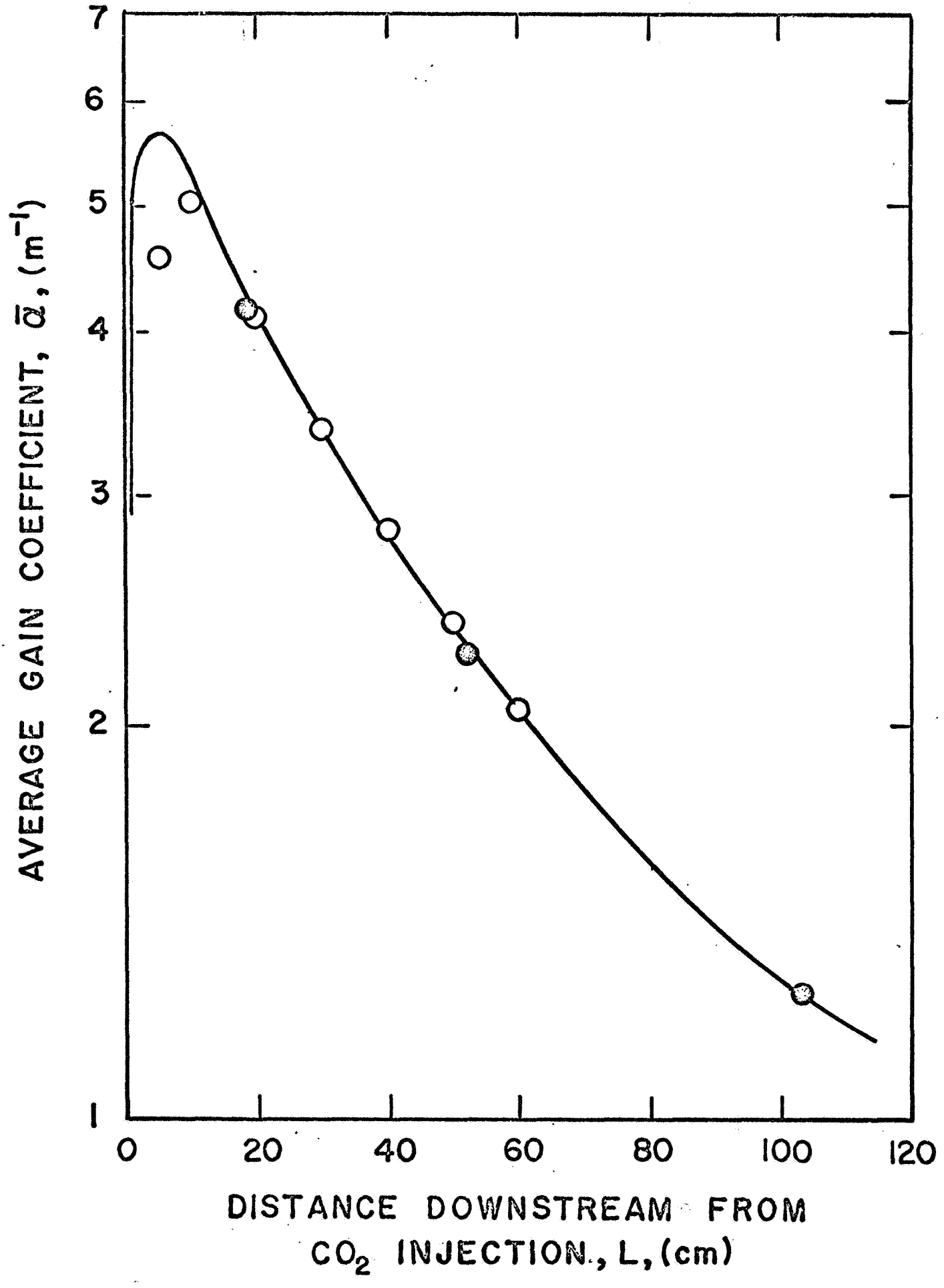
AVERAGE GAIN COEFFICIENT, $\bar{\alpha}$, (m^{-1})
7
6
5
4
3
2
1
0
20
40
60
80
100
120
DISTANCE DOWNSTREAM FROM
CO_2 INJECTION., L, (cm)

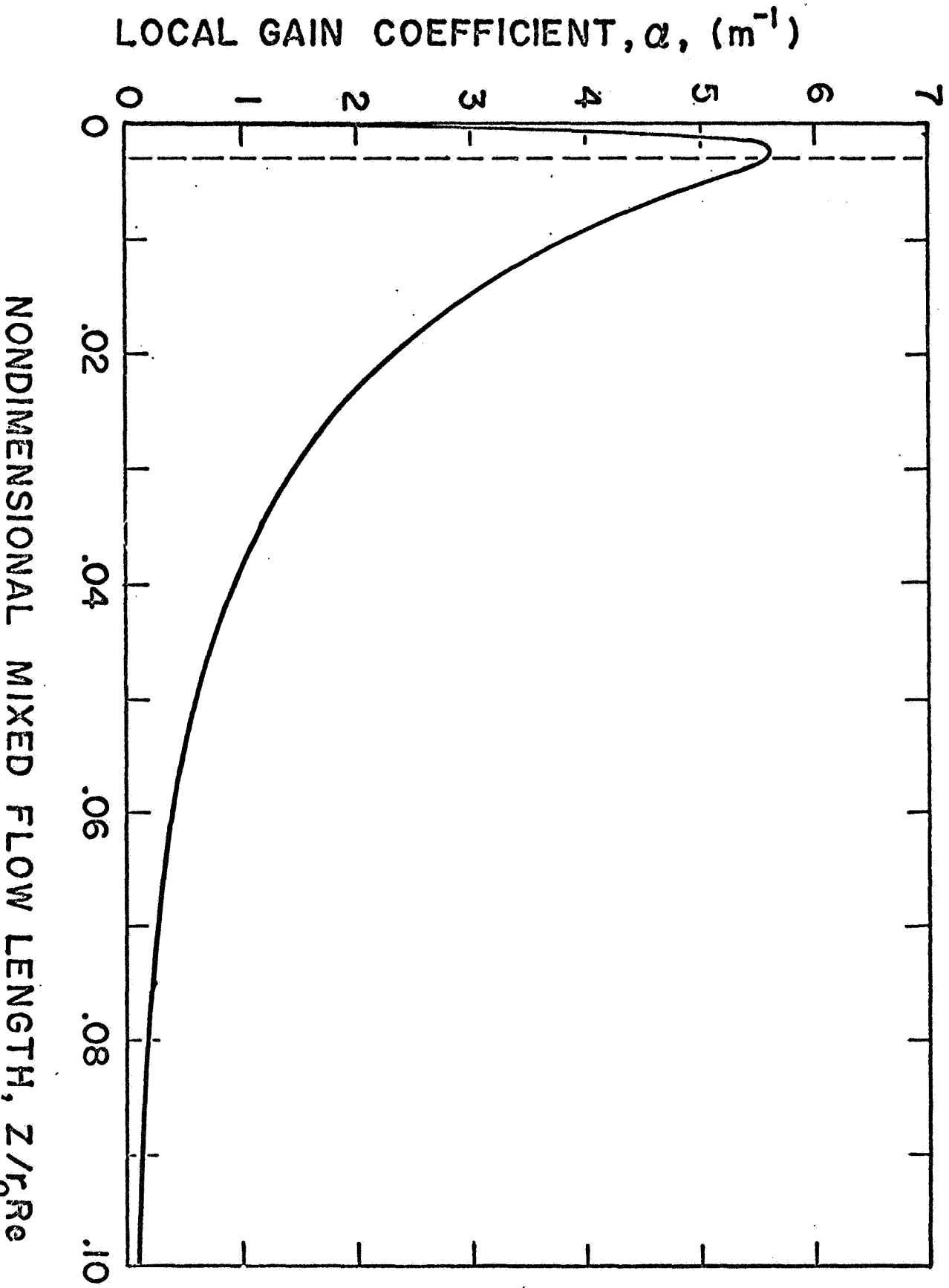
LOCAL GAIN COEFFICIENT, α, (m^{-1})
0
1
2
3
4
5
6
7
0
.02
.04
.06
.08
.10
NONDIMENSIONAL MIXED FLOW LENGTH, Z/r_0Re

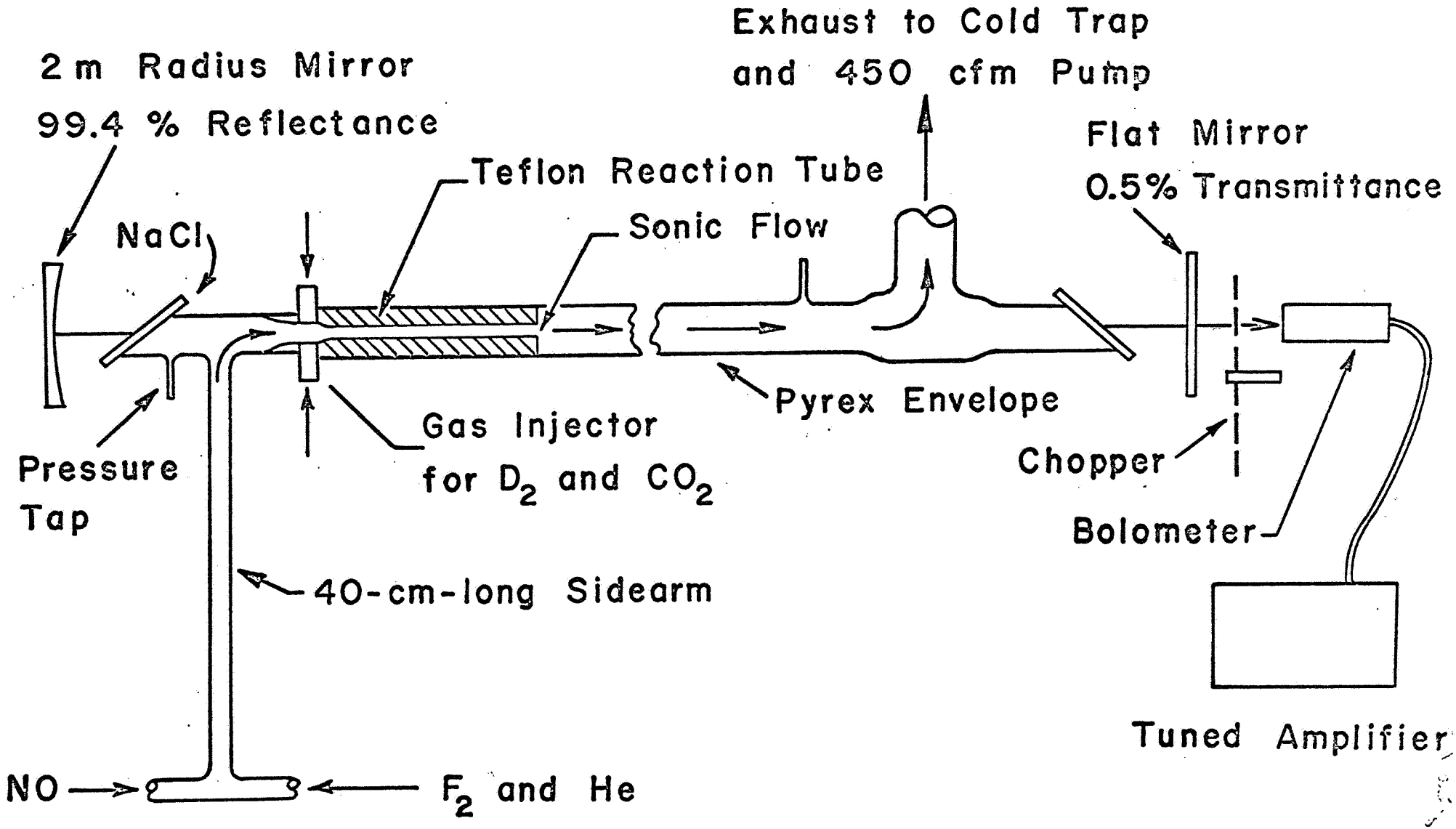
Exhaust to Cold Trap
and 450 cfm Pump
2 m Radius Mirror
99.4 % Reflectance
Flat Mirror
0.5% Transmittance
Teflon Reaction Tube
Sonic Flow
NaCl
Pressure
Tap
Gas Injector
for D_2 and CO_2
Pyrex Envelope
Chopper
Bolometer
40-cm-long Sidearm
NO
F_2 and He
Tuned Amplifier

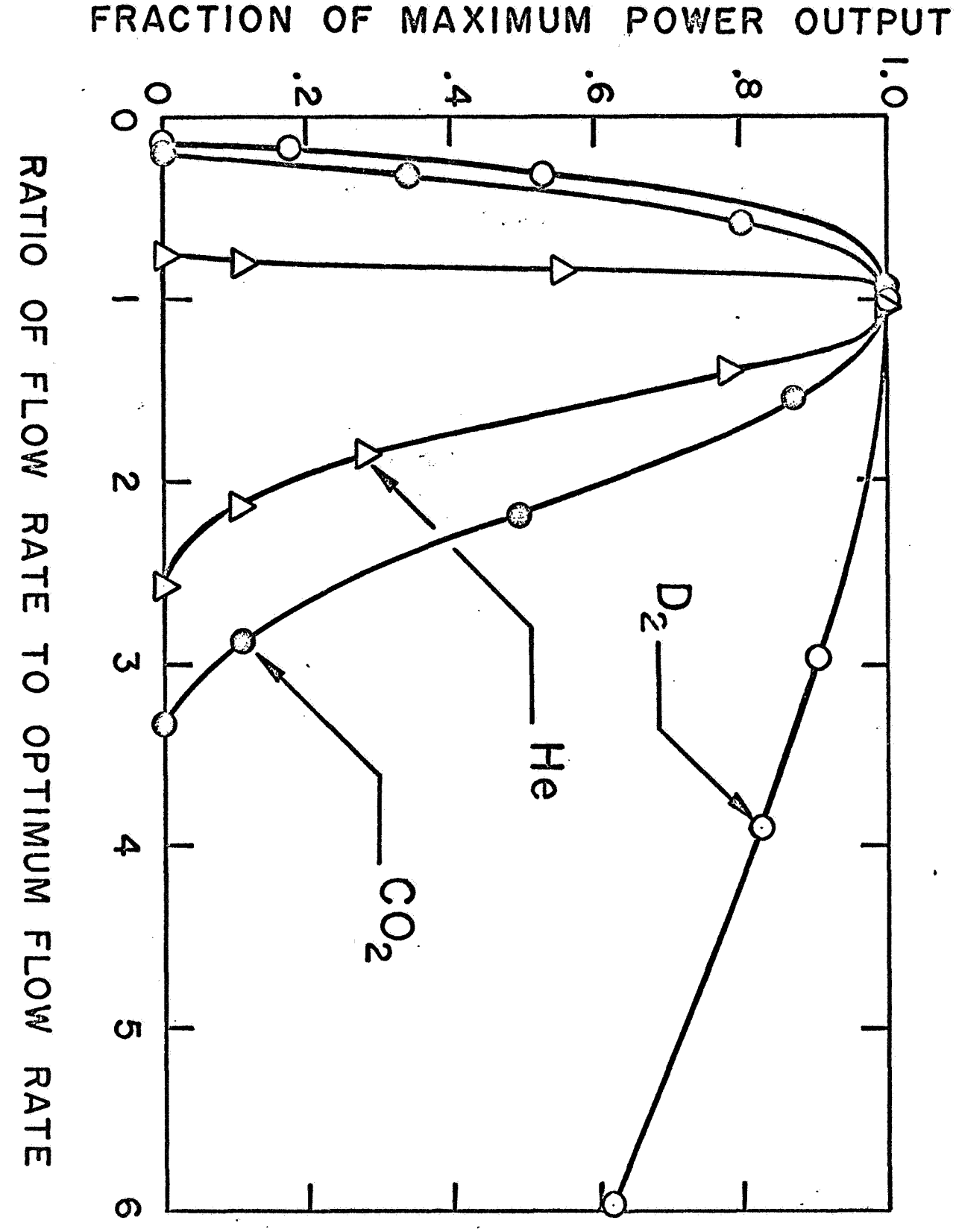
FRACTION OF MAXIMUM POWER OUTPUT
0
.2
.4
.6
.8
1.0
RATIO OF FLOW RATE TO OPTIMUM FLOW RATE
0
1
2
3
4
5
6
CO_2
He
D_2

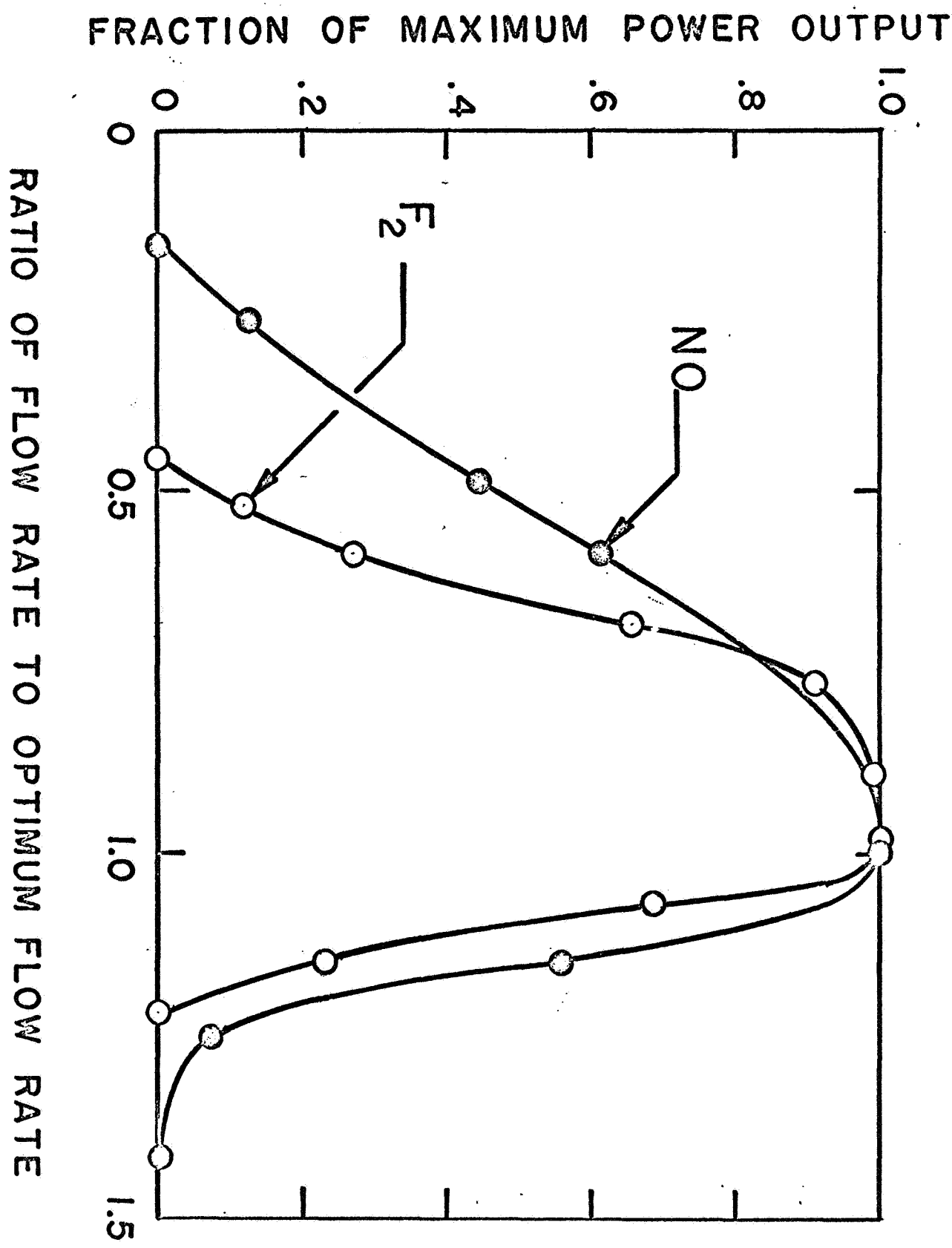
FRACTION OF MAXIMUM POWER OUTPUT
0
.2
.4
.6
.8
1.0
RATIO OF FLOW RATE TO OPTIMUM FLOW RATE
0
0.5
1.0
1.5
F2
NO

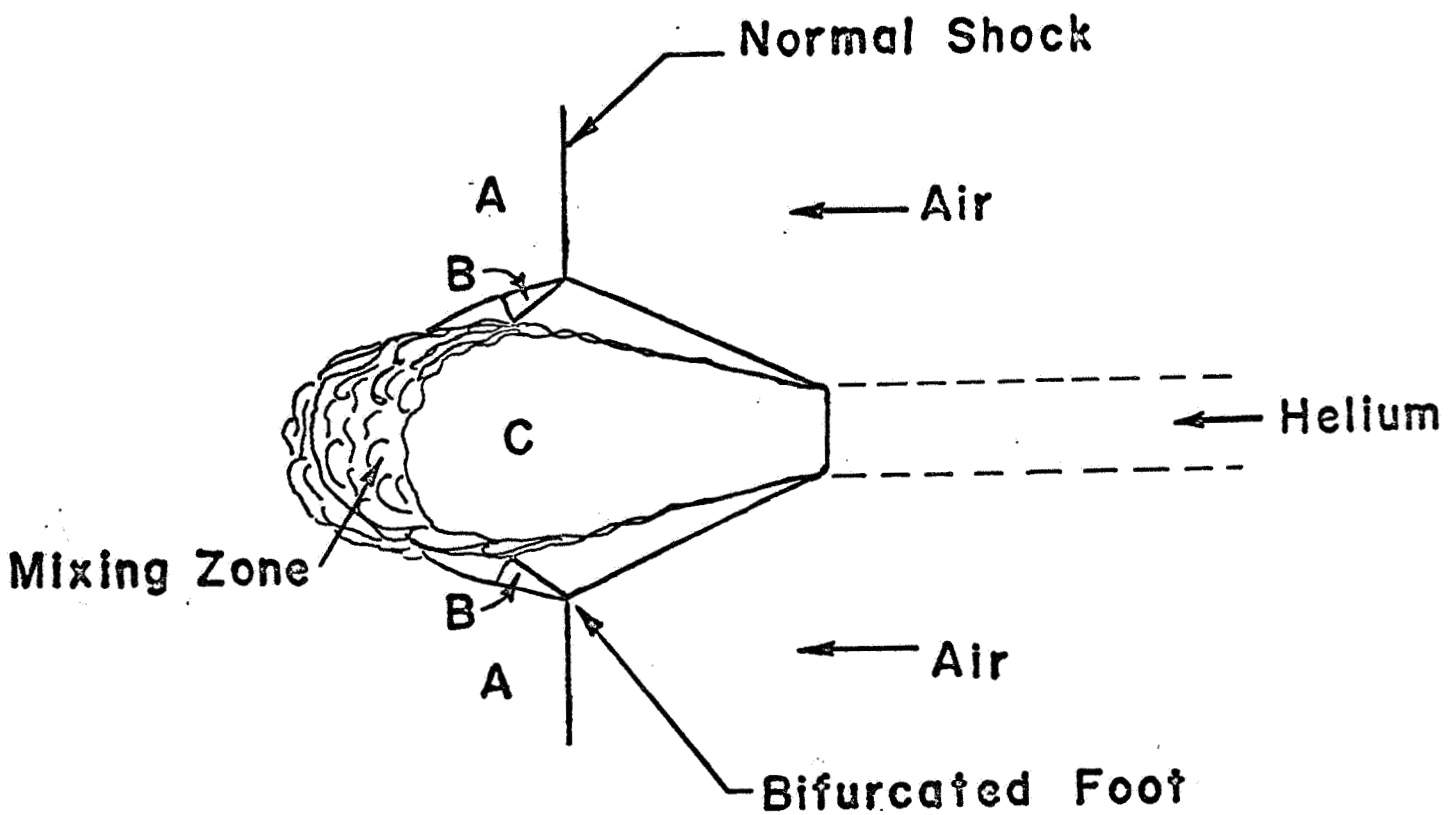
Normal Shock
A
Air
B
C
Helium
Mixing Zone
B
Air
A
Bifurcated Foot

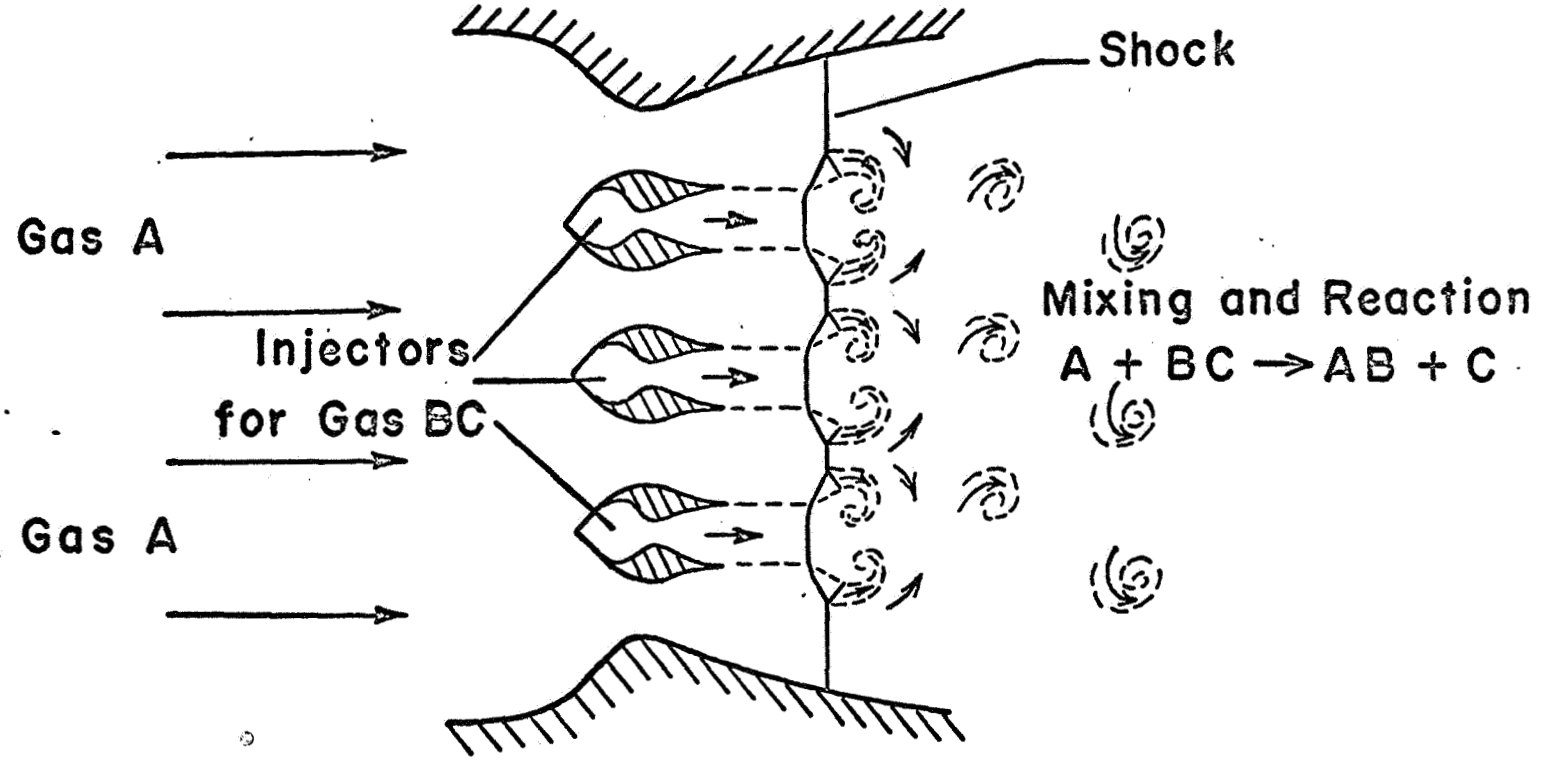

SHOCK MIXING AND REACTION